

# **I. Project Research**

## **Project 5**

Y. Sakurai

*Institute for Integrated Radiation and Nuclear Science,  
Kyoto University*

#### BACKGROUNDS AND PURPOSES:

There are a number of subjects, which should be improved for the further advance and generalization of boron neutron capture therapy (BNCT). In the viewpoints of medical physics and engineering, the advance for dose estimation is one of the important subjects. The purposes of this project research are the advance for various dose estimation methods, and the establishment of an integrated system for dose estimation in BNCT.

In the third year of this research project, 2019, the advancement for the respective dose estimation methods were forwarded mainly using Heavy Water Neutron Irradiation Facility (HWNIF) and E-3 Neutron Guide Tube (E-3) at KUR, sequentially the previous year. In addition, the integrated system was considered for the simultaneous usage of several dose estimation methods.

#### RESEARCH SUBJECTS:

The collaboration and allotted research subjects (ARS) were organized as follows;

- ARS-1 (31P5-1):** Establishment of characterization estimation method in BNCT irradiation field using Bonner sphere and ionization chamber (III). (Y. Sakurai, S. Shiraiishi, N. Matsubayashi, K. Okazaki, A. Sasaki, Y. Kumagai, T. Naito, T. Nakamura, Y. Kakimoto, H. Matsunaga, T. Takata and H. Tanaka)
- ARS-2 (31P5-2):** Study on new type of neutron spectrometer for BNCT. (A. Uritani, A. Ishikawa, K. Watanabe, S. Yoshihashi, A. Yamazaki and Y. Sakurai)
- ARS-4 (31P5-4):** Neutron measurement by using the self-activation of iodine-added plastic scintillators. (A. Nohtomi, Y. Hanada, G. Wakabayashi, Y. Sakurai and T. Takata)
- ARS-5 (31P5-5):** Characterization of active neutron detector for boron neutron capture therapy. (M. Takada, S. Endo, H. Tanaka, T. Matsumoto, A. Masuda, T. Nunomiya, K. Aoyama and T. Nakamura)
- ARS-6 (31P5-6):** Study for microdosimetry using silicon-on-insulator microdosimeter in the BNCT irradiation field (III). (Y. Sakurai, N. Ko, T. Takata, H. Tanaka, T. L. Tran, J. Davis, S. Guatelli, A. Rozenfeld, N. Kondo and M. Suzuki)
- ARS-7 (31P5-7):** Measurement of BNCT beam component fluence with polymer gel detector. (K. Tanaka, Y. Sakurai, T. Kajimoto, Y. Ito, H. Tanaka, T. Takata and S. Endo)
- ARS-8 (31P5-8):** Development of neutron fluence distribution measuring device using Thermoluminescence slabs. (K. Shinsho, R. Oh, M. Tanaka, S. Yanagisawa, H. Tanaka, T. Takata, G. Wakabayashi and Y. Koba)
- ARS-9 (31P5-9):** The study for development and application of tissue equivalent neutron dosimeter. (M. Oita, T. Kamomae, T. Takada and Y. Sakurai)
- ARS-10 (31P5-10):** Development and evaluation of 3D gel dosimeter for the measurement of dose distribution in BNCT. (S. Hayashi, Y. Sakurai, M. Suzuki and T. Takata)
- ARS-11 (31P5-11):** Establishment of beam-quality estimation method in BNCT irradiation field using dual phantom technique (III). (Y. Sakurai, T. Takata, H. Tanaka, N. Kondo and M. Suzuki)
- ARS-12 (31P5-12):** Characteristics test of a prompt gamma-ray detector using LaBr<sub>3</sub>(Ce) scintillator and 8×8 array MPPC for boron neutron capture therapy. (K. Okazaki, K. Akabori, T. Takata, S. Kawabata, Y. Sakurai and H. Tanaka)
- ARS-13 (31P5-13):** Development of fiber-reading radiation monitoring system with a red/infrared-emitting scintillator at <sup>60</sup>Co radiation facilities. (S. Kurosawa, S. Kodama, T. Takada, Y. Sakurai and H. Tanaka)
- ARS-14 (31P5-14):** Establishment of the imaging technology of 478 keV prompt gamma-rays of boron-neutron capture reaction and the measurement of the intensity of the neutron field. (T. Mizumoto, S. Komura, Y. Sakurai, A. Takada, T. Takata and T. Tanimori)
- ARS-15 (31P5-15):** Feasibility study of a gel-dosimeter for a quality assurance and a quality control in boron neutron capture therapy. (S. Nakamura, K. Iijima, M. Takemori, H. Nakayama, S. Nishioka, H. Okamoto, Y. Sakurai, H. Tanaka, T. Takata, M. Suzuki, H. Igaki and J. Itami)
- ARS-16 (31P5-16):** Optimization of bolus shape for boron neutron capture therapy using epi-thermal neutron beam. (T. Takata, H. Tanaka, A. Sasaki, Y. Sakurai, A. Maruhashi and M. Suzuki)
- ARS-17 (31P5-17):** Development of novel radiochromic gels for assessing 3-dimensional dose distribution in brain. (H. Yasuda, J.E. Tano, C.A.B. Gonzales and Y. Sakurai)
- ARS-18 (31P5-18):** Measurement of neutron distributions in the BNCT irradiation field using a GEM detector. (S. Uno, T. Koike, K. Miyamoto, K. Nobori and H. Tanaka)
- ARS-20 (31P5-20):** Development of epi-thermal neutron flux intensity detector for BNCT. (I. Murata, K. Aoki, Y. Miyaji, S. Kusaka, H. Tanaka, Y. Sakurai and T. Takada)
- ARS-21 (31P5-21):** Investigation of thermal neutron-induced soft errors in semiconductor devices. (H. Tanaka, T. Kato, H. Matsuyama, T. Takata and Y. Sakurai)

For ARS-3, no results were obtained because the insufficient neutron intensities of HWNIF for this subject. For ARS-19, the animal experiments at E-3 were originally planned but could not be performed, because the registration of E-3 as an animal experimental room was not in time. So, the reports of these subjects are not appeared.

## PR5-1-1 Establishment of characterization estimation method in BNCT irradiation field using Bonner sphere and ionization chamber (III)

Y. Sakurai, S. Shiraishi<sup>1</sup>, N. Matsubayashi<sup>1</sup>, K. Okazaki<sup>1</sup>, A. Sasaki<sup>1</sup>, Y. Kumagai<sup>1</sup>, T. Naito<sup>1</sup>, T. Nakamura<sup>1</sup>, Y. Kakimoto<sup>1</sup>, H. Matsunaga<sup>1</sup>, T. Takata, H. Tanaka

*Institute for Integrated Radiation and Nuclear Science,  
Kyoto University*

<sup>1</sup>*Graduate School of Engineering, Kyoto University*

<sup>2</sup>*Osaka Medical School*

**INTRODUCTION:** Research and development into several types of accelerator-based irradiation systems for boron neutron capture therapy (BNCT) is underway [1,2]. In the near future, BNCT using these newly developed irradiation systems may be carried out at multiple facilities across the world. Considering this situation, it is important that the estimations for dose quantity and quality are performed consistently among several irradiation fields, and that the equivalency of BNCT is guaranteed, within and across BNCT systems. Then, we are establishing the quality assurance and quality control (QA/QC) system for BNCT irradiation field.

As part of the QA/QC system, we are developing estimation method for neutron energy spectrum using Bonner sphere [3]. For our spectrometer using Bonner sphere, liquid such as pure water and/or boric acid solution is used as the moderator. A multi-layer concentric-sphere case with several sphere shells is prepared. The moderator and its diameter are changeable without entering the irradiation room, by the remote supply and drainage of liquid moderator in the several layers. For the detector, activation foils are remotely changed, or online measurement is performed using SOF (scintillator with optical fiber) detector containing boron, etc. [4].

In 2019, a prototype of the Remote-changeable Bonner-sphere Spectrometer (RBS) was made. An experiment was performed for the characteristic verification of the prototype RBS at Heavy Water Neutron Irradiation Facility of Kyoto University Reactor (KUR-HWNIF).

**METHODS:** In the neutron energy spectrometry by Bonner-sphere, the combinations of the moderator material and diameter should be previously decided and prepared. Of course, the more information can be obtained as the more moderators and detectors are prepared. However, the information number from those measured data is less than the combination number, because of the overlapped regions among the combinations. The selection is important, in which the more information number is obtained for the combination number.

The combination of moderator and detector is decided, for that the response functions cannot be approximated by the linear functions of the other response functions. The accuracy and precision for the spectrometry can be higher, because the independent information can be obtained from the measurement by the respective combinations. We were developed the selection method, High

Independence Selection (HIS) [5].

On the assumption of the application in the standard epi-thermal neutron irradiation mode of KUR-HWNIF, the combination of the moderators for boron-10 concentration and diameter was optimized by HIS. Based on this optimization, a configuration of an RBS was decided and a prototype of RBS was made. An experiment was performed for the characteristic verification of the prototype RBS in the standard epi-thermal neutron irradiation mode of KUR-HWNIF.

**RESULTS:** The configuration of the RBS was decided as follows. A five-layer concentric spherical acrylic shell is used as a container. Each acrylic wall is 1 mm in thickness. The moderator injection part is 9 mm in thickness for each layer. Pure water and 0.15-weight-percent boric acid water for boron-10 (45 g/l solubility for H<sub>3</sub>BO<sub>3</sub> at 20 degree Centigrade) were used as liquid moderators. A LiCaF scintillation detector is used.

Figure 1 shows an example of the optimized combination of moderator injection patterns for RBS. Photo 1 shows a prototype RBS, which was made based on the optimization. It was confirmed that the experimental results were in good agreement with the simulation results for the ratios of the detector responses for the respective moderator injection patterns.

**CONCLUSION:** We plan to further analyze the experimental data, and improve the prototype RBS.

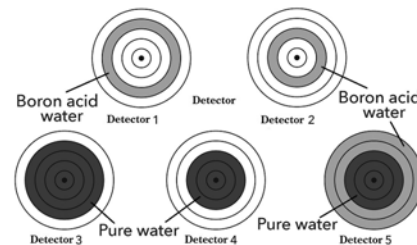


Fig. 1. An example of the optimized combination of moderator injection patterns for RBS.



Photo 1. A prototype RBS.

### REFERENCES:

- [1] H. Tanaka *et al.*, Nucl. Instr. Meth. B **267** (2009) 1970-1977.
- [2] H. Kumada *et al.*, Appl. Radiat. Isot. **88** (2014) 211-215.
- [3] H. Ueda *et al.*, Appl. Radiat. Isot. **104** (2015) 25-28.
- [4] M. Ishikawa *et al.*, Radiat. Oncol. **11** (2016) 105(1-10).
- [5] H. Ueda, Doctoral Thesis (2016).

A. Uritani, A. Ishikawa, K. Watanabe, S. Yoshihashi, A. Yamazaki and Y. Sakurai<sup>1</sup>

Graduate School of Engineering, Nagoya University  
<sup>1</sup> Institute for Integrated Radiation and Nuclear Science, Kyoto University

**INTRODUCTION:** Boron neutron capture therapy (BNCT) is a promising treatment method for cancers such as brain tumors. Recently, an accelerator-driven neutron source has actively been developed owing to its simplicity of management. In commissioning phase of the facilities, specifications of the irradiation field, such as neutron intensity, the neutron energy spectrum and gamma-ray contamination, should be characterized in order to assure designed ones.

We are developing a new neutron energy spectrometer using the optical fiber type detector. The conventional technique for neutron spectrometry is the Bonner sphere method. Generally, moderation based neutron spectrometers should be improved in energy response especially for epi-thermal neutron energy region. In order to improve the energy response, the number of detectors with different responses should be increased. We propose the spectrometer consisting of liquid moderator and thermal neutron flux profile scanner using the optical fiber type detector. So far, we has developed the optical fiber type detector showing a neutron peak in the pulse height spectrum [1]. The detector used the Eu:LiCaAlF<sub>6</sub> scintillator, which has relatively slow decay time of 1.6  $\mu$ s. In order to expand the dynamic range of the neutron detector, it is desired to use faster scintillator to improve the counting rate capability. As a fast neutron scintillator, the Li glass scintillator is well known. However, the light yield of the Li glass is quite low compared with the Eu:LiCaAlF<sub>6</sub> scintillator. Therefore, it was considered to be difficult to fabricate the optical fiber type detector showing a neutron peak.

**EXPERIMENTS:** We fabricated the optical fiber type neutron detector using Li glass scintillator. A small piece of the Li glass scintillator was mounted at a tip of the optical fiber. The scintillator was coated with a reflector powder and then covered with a heat shrinkin tube for light shielding. Figure 1 shows the fabrication procedure of the optical fiber type detector using the Li glass scintillator.

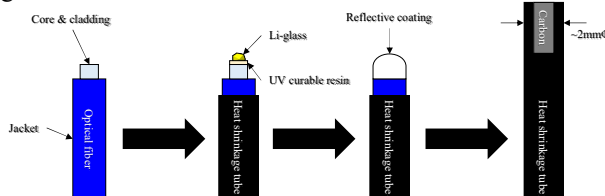


Fig. 1. Fabrication procedure of the optical fiber type detector using the Li glass scintillator.

First of all, we evaluated the detector response at the E3 port of the Kyoto University Reactor. And then, the fab-

ricated detector was irradiated with intense neutrons with the flux of  $4 \times 10^8$  n/cm<sup>2</sup>/s at Heavy Water Irradiation Facility of Kyoto University Reactor.

**RESULTS:** Figure 1 shows pulse height spectrum obtained from the fabricated optical fiber type detector using the Li glass scintillator. The detector shows a clear neutron peak. This is because a high NA optical fiber is used in the detector. The high NA optical fiber helps to efficiently collect scintillation photons from low light yield scintillator.

Figure 2 shows the time trend of the neutron peak channel during irradiation with intense neutrons with the flux of  $4 \times 10^8$  n/cm<sup>2</sup>/s. No significant deterioration of the signal gain was confirmed. Since the fabricated detector used the silica fiber, the detector is considered to show sufficient radiation hardness.

#### REFERENCES:

- [1] K. Watanabe *et al.*, Nuclear Instruments and Methods in Physics Research Section A, **802**, 1 (2015).

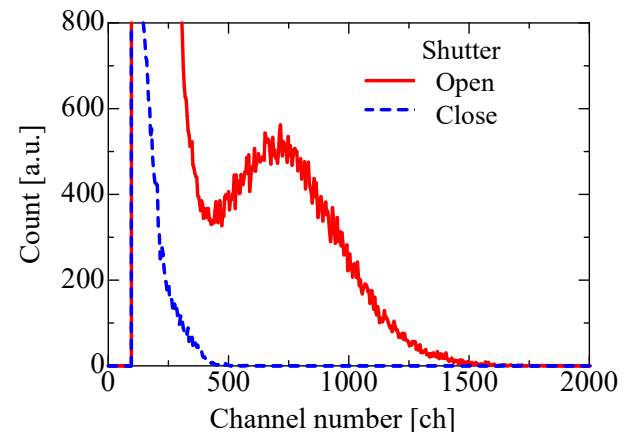


Fig. 2. Pulse height spectrum obtained from the optical fiber neutron detector using the Li glass scintillator.

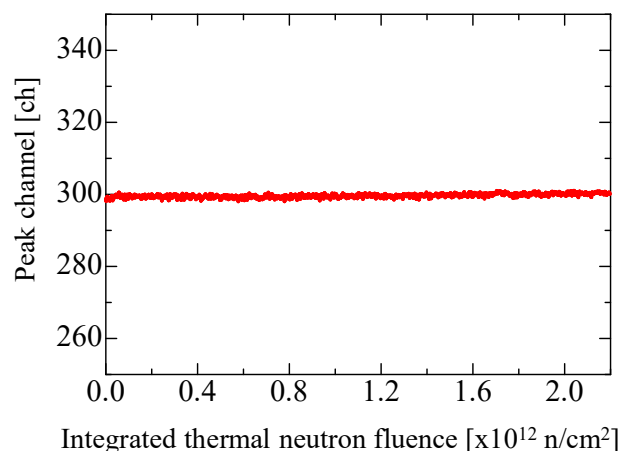


Fig. 3. Time trend of the neutron peak channel during irradiation with intense neutrons with the flux of  $4 \times 10^8$  n/cm<sup>2</sup>/s.

## PR5-33 Neutron measurement by using the self-activation of iodine-added plastic scintillators

A. Nohtomi, Y. Hanada, G. Wakabayashi<sup>1</sup>, Y. Sakurai<sup>2</sup> and T. Takata<sup>2</sup>

Graduate School of Medicine, Kyushu University

<sup>1</sup> Atomic Energy Research Institute, Kindai University

<sup>2</sup> Institute for Integrated Radiation and Nuclear Science, Kyoto University

**INTRODUCTION:** In our previous works, thermal neutron was measured by using the self-activation of iodine-containing inorganic scintillators such as NaI and CsI [1, 2]. The method is highly sensitive even for short time irradiation, but not appropriate for very intense neutron field like the BNCT treatment, because the tuning of sensitivity is not possible. Another drawback is the production of byproduct activity, <sup>24</sup>Na and <sup>134m</sup>Cs. In the present work, the applicability of iodine-added plastic scintillator was studied at rather intense neutron field like BNCT one of KUR irradiation facility

**EXPERIMENTS:** Iodine-added plastic scintillator was fabricated with an optical modeling type 3D printer (MiiCraft: MiiCraft Corp.). The base component was M211-B and PPO; small amount of Bis-MSB and Irgacure TPO are also mixed. In addition, iodobenzene (C<sub>6</sub>H<sub>5</sub>I) was added to the base material of plastic scintillator by 1 wt% and 0.1 wt% (Fig.1). Two plastic scintillators were irradiated at Rail Device of the Heavy Water Neutron Irradiation Facility with OO-0000F mode (1MW) [3]. Those scintillators were put at the Bismuth Surface (thermal neutron flux : ~10<sup>9</sup> n/cm<sup>2</sup>/s) during 10 seconds for 1 wt% scintillator and 100 seconds for 0.1 wt% one. After the termination of each irradiation, the output signal of scintillators was read out by PMT and MCA every one minute continuously.

**RESULTS:** Figure 2 shows pulse height distributions observed by the two iodine-added plastic scintillators: 1 wt% and 0.1 wt%. Reference spectrum of <sup>128</sup>I beta-rays is also indicated for comparison. Although iodobenzene is known one of the strongest chemical quenchers, the shift of pulse-height distribution towards low energy region is not so significant because the amount added to plastic scintillator is very small, but negligible.



Fig. 1. Appearance of iodine-added plastic scintillator. (diameter : 25 mm, height : 25 mm)

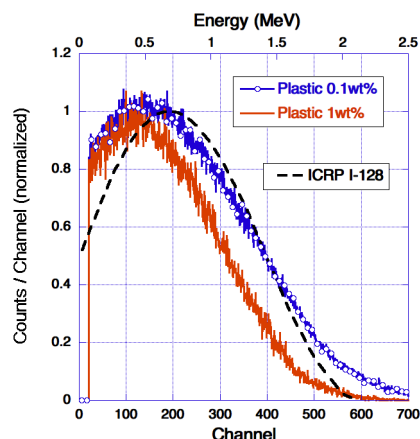


Fig. 2. Pulse height distributions observed by the iodine-added plastic scintillators.

Figure 3 shows decay curves of count rate observed by the iodine-added plastic scintillators. Only <sup>128</sup>I decaying components with half-life of 25 min are seen for both 1 wt% and 0.1 wt% scintillators. As clearly indicated in the figure, no byproduct radio-activity is produced. This property is very desirable for the application of iodine-added plastic scintillator to intense BNCT neutron field.

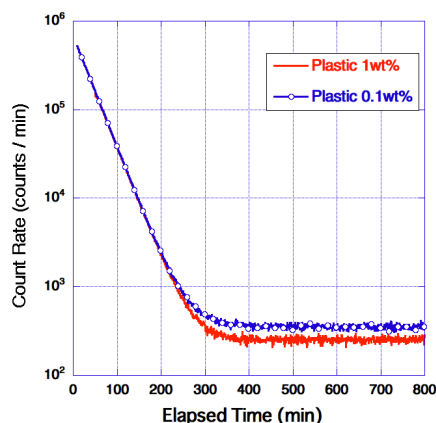


Fig. 3. Decay curves of count rate observed by the iodine-added plastic scintillators.

**ACKNOWLEDGEMENT:** This work was supported by JSPS KAKENHI Grant Number JP19K08202.

Dr. T. Kin and Mr. Y. Shinjyo of Kyushu University are deeply appreciated for their fabrication of iodine-added plastic scintillators.

### REFERENCES:

- [1] G. Wakabayashi *et al.*, Radiol. Phys. Technol., **8** (2015) 125-134.
- [2] A. Nohtomi *et al.*, JPS Conf. Proc., **24** (2019) 011041.
- [3] Y. Sakurai and T. Kobayashi, Nucl. Instr. and Meth., **A453** (2000) 569-596.

## PR5-4-4 Characterization of Active Neutron Detector for Boron Neutron Capture Therapy

M. Takada, S. Endo<sup>1</sup>, H. Tanaka<sup>2</sup>, T. Matsumoto<sup>3</sup>,  
A. Masuda<sup>3</sup>, T. Nunomiya<sup>4</sup>, K. Aoyama<sup>4</sup>, T. Nakamura<sup>4</sup>

Department of Applied Physics, National Defense  
Academy of Japan

<sup>1</sup>Graduate School of Engineering, Hiroshima University

<sup>2</sup>Institute for Integrated Radiation and Nuclear Science,  
Kyoto University

<sup>3</sup>National Metrology Institute of Japan, National Institute  
of Advanced Industrial Science and Technology

<sup>4</sup>Fuji Electric Co. Ltd.

**INTRODUCTION:** Boron Neutron Capture Therapy (BNCT) is a binary radiotherapy method developed to treat patients with certain malignant tumors. BNCT has been widely used at nuclear reactors. Recently, several accelerator-based BNCT facilities have been developed, or ready to clinical treatment for more accessible for patients. Intensity of neutron beam produced from the neutron accelerator could be varied with time due to instability of the accelerator condition and the neutron target degeneration. The neutron beam should be continuously measured in a real time.

The active neutron detector, which composes of thin silicon sensor with a 40  $\mu\text{m}$  thickness and ultra thin LiF neutron converter with around 0.1  $\mu\text{m}$  thickness, have been developed to measure the BNCT neutron beam. Using this neutron detector, intense neutron beam over  $1 \times 10^9 \text{ (cm}^{-2} \text{ s}^{-1}\text{)}$  and high dose-rate gamma rays around 500 mGy/h were measured separately at the two BNCT facilities in KURNS (Institute for Integrated Radiation and Nuclear Science, Kyoto University) and NCC (National Cancer Research Center) [1-3]. Although it is said that the silicon detector is sensitive to neutron irradiation, no neutron damage have been observed.

At the NCC BNCT neutron facility, relative neutron depth distribution in an acrylic block was measured. The neutron detection efficiency is required to evaluate absolute neutron depth distribution. In this study, the detection efficiency of the real-time neutron detector for thermal neutron was experimentally obtained.

In the BNCT neutron beam, fast neutron component is included other than thermal neutrons. The patients could be affected by fast neutrons. The fast neutron component is preferred to be measured in addition to thermal neutron measurement. In this study, the fast neutron components were measured by exchanging the LiF neutron converter to polyethylene sheet. The 30- $\mu\text{m}$ -thick thin silicon sensor was applied to deduce another gamma sensitivity.

**EXPERIMENTS:** The neutron measurements were performed at the heavy water irradiation facility of research reactor of KURNS. The neutron detector was located in the center of neutron beam area. Signals from the neutron sensor were fed to a preamplifier outside of the irradiation room, and then, acquired using fast digital pulse-shaping processor. The thermal neutron beam fluxes and cadmium ratios are changed by opening a Cd

aperture slit at an upward of the irradiation location. Neutron flux at the irradiation position was, also, measured using gold neutron activation analysis. In the measurements of fast neutrons, the fast neutron detector was located at the same positions as the thermal neutron detector. The Cd slit was closed to decrease the thermal neutron flux. The thickness of depletion layer was changed with bias voltages.

**RESULTS:** The response functions normalized with the thermal neutron flux, which was evaluated from the gold neutron activation analysis, were obtained. The neutron peak in the response function is created by detecting triton events produced from the  $n\text{-}^6\text{Li}$  reaction. The detection efficiency for thermal neutron was experimentally obtained by integrating the neutron peak counts. The neutron detection efficiency was evaluated,  $3.5 \times 10^{-5} \text{ (cm}^{-2}\text{)}$ . This results will be used to evaluate the absolute neutron depth distribution.

The pulse heights detecting the fast neutron were shown in **Fig.1**. The measurements show edges around 1100 ch, indicated by an arrow. Events from 500 ch to 1400 ch are created by detecting protons recoiled by fast neutrons at polyethylene converter. Black, red, and light green solid line show the measurement results, applying the bias voltage, -4, -0.5, and 0V, respectively. The -4 V voltage creates the thickest depletion layer. These edge positions are dependent on bias voltage, equivalent to thickness of depletion layer. Without polyethylene converter, this edge was not observed, shown as a blue solid line. From this result, fast neutron components in the BNCT neutron beam can be measured.

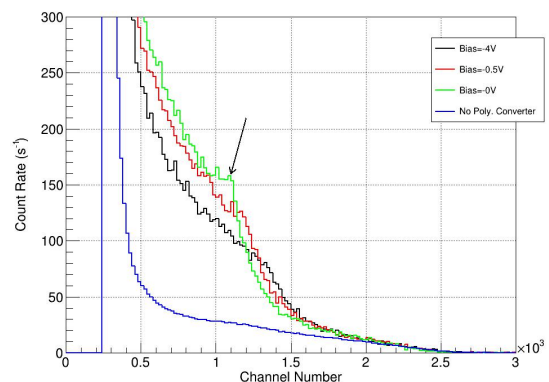


**Figure 1. Pulse heights detecting fast neutrons, using thin Si detector attached with a polyethylene neutron converter and applied with several bias voltages, compared to measurement without neutron converter.**

### REFERENCES:

- [1] M. Takada *et al.*, Radiat. Meas., 99, 33-54 (2017).
- [2] M. Takada *et al.*, Appl. Radiat. Isotopes (submitted).
- [3] M. Takada *et al.*, Radiat. Meas. (submitted).

Y. Sakurai<sup>1</sup>, N. Ko<sup>1,2</sup>, T. Takata<sup>1</sup>, H. Tanaka<sup>1</sup>, T. L. Tran<sup>3</sup>, J. Davis<sup>3</sup>, S. Guatelli<sup>3</sup>, A. Rozenfeld<sup>3</sup>, N. Kondo<sup>1</sup>, M. Suzuki<sup>1</sup>

<sup>1</sup>Institute for Integrated Radiation and Nuclear Science, Kyoto University

<sup>2</sup>Kansai BNCT Medical Center, Osaka Medical College

<sup>3</sup>Centre for Medical Radiation Physics, University of Wollongong

**INTRODUCTION:** Research and development into several types of accelerator-based irradiation systems for boron neutron capture therapy (BNCT) is underway [1,2]. In the near future, BNCT using these newly developed irradiation systems may be carried out at multiple facilities across the world. In contrast to conventional radiotherapy, the types of radiation present in BNCT consists of many distinct radiation components, each having a different biological weighting factor.

Microdosimetry is an effective dosimetry technique in a mixed radiation environment. Using this technique, it is possible to derive the relative contributions of different radiation modalities. The feasibility study of a novel 3D mesa bridge silicon-on-insulator microdosimeter (SIM) in BNCT [3], developed by University of Wollongong (UOW).

In 2019, a new design silicon microdosimeter and its use for dosimetry in boron neutron capture therapy (BNCT) were investigated by Monte Carlo simulation.

**METHODS:** Two detector configurations were investigated, based on the current 3D mushroom microdosimeter. The first structure consists of a cylindrical p+ core electrode through the center of the SV with n+ ring electrode wrapped around the outside of the SV. The second structure consists of a cylindrical n+ core electrode through the center of the SV with p+ ring electrode wrapped around the outside of the SV. Each SV has a diameter and height of 10  $\mu\text{m}$  and the pitch between each individual SV is 40  $\mu\text{m}$  to reduce cross talk between neighboring row of detectors. A total of 2500 individual SVs were connected in an array with odd and even detector row readout channels.

PHITS was used for this study. The T-deposit tally, which scores dose and event-by-event deposition energy distribution was used to calculate the energy deposited inside the SV of the mushroom microdosimeter. The microdosimetric spectrum (frequency mean and dose mean lineal energy distribution) were calculated by dividing the deposited energy by the average chord length of the SV. The detectors response to neutrons were investigated using the neutron source for the mixed neutron irradiation of Heavy Water Neutron Irradiation Facility installed in Kyoto University Reactor (KUR-HWNIF).

**RESULTS:** The deposit energy spectrum obtained with

the p+ core and p+ ring detector when irradiated by the mix irradiation mode of KUR-HWNIF are shown in Figs. 1 and 2, respectively. Higher events were observed with the p+ ring detector, due to the larger surface area of the p+ region (i.e. absolute number of  $^{10}\text{B}$  atoms were larger). The dominant component was the 1.47 MeV alpha particle, followed by the 840 keV  $^7\text{Li}$  ion. A small amount of recoil silicon was observed. The lineal energy was calculated and the  $yd(y)$  versus  $\log(y)$  distribution was calculated, as shown in Fig. 3. From this spectrum, the p+ core design had a higher lineal energy than the p+ ring and the previous version microdosimeter (3D bridge).

**CONCLUSION:** It was confirmed that the new detector can accurately measure the lineal energy of alpha particles emitted from the  $^{10}\text{B}(n,\alpha)^7\text{Li}$  reaction.

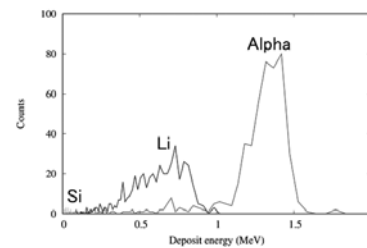


Fig. 1. Deposit energy spectrum for the p+ core.

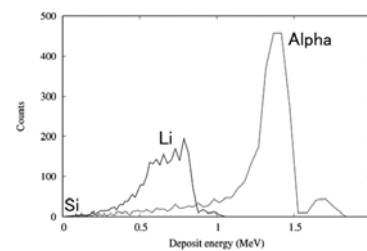


Fig. 2. Deposit energy spectrum for the p+ ring.

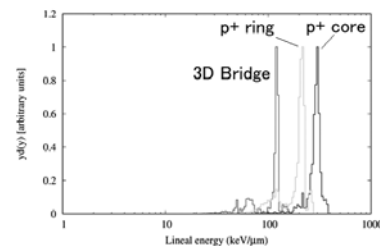


Fig. 3. Microdosimetric  $yd(y)$  spectrum of the p+ core and p+ ring detector, normalised to maximum.

#### REFERENCES:

- [1] H. Tanaka *et al.*, Nucl. Instr. Meth. B **267** (2009) 1970-1977.
- [2] H. Kumada *et al.*, Appl. Radiat. Isot. **88** (2014) 211-215.
- [3] L. T. Tran *et al.*, IEEE Trans. Nucl. Sci. **62** (2015) 3027-3033.

## PR5-6 Measurement of BNCT beam component fluence with polymer gel detector

K. Tanaka, Y. Sakurai<sup>1</sup>, T. Kajimoto, Y. Ito, H. Tanaka<sup>1</sup>,  
T. Takata<sup>1</sup>, S. Endo

Graduate School of Engineering, Hiroshima University  
<sup>1</sup> Institute for Integrated Radiation and Nuclear Science,  
Kyoto University

**INTRODUCTION:** Evaluation of dose is required for quality assurance in the irradiation field used for boron neutron capture therapy. This study investigated the use of the MAGAT polymer gel detector in the QA by estimation of dose and position resolution.

**EXPERIMENTS:** The experiment was performed with the standard epithermal neutron irradiation mode of KUR-HWNIF at 1 MW. The beam size was set to about  $120 \times 120 \text{ mm}^2$  using the collimator. The irradiation was performed for 2 minutes. The nominal value of the flux at the center of the collimator aperture was  $7.07 \times 10^6 \text{ cm}^{-2}\text{s}^{-1}$ ,  $1.33 \times 10^8 \text{ cm}^{-2}\text{s}^{-1}$  and  $1.38 \times 10^7 \text{ cm}^{-2}\text{s}^{-1}$  for thermal, epithermal and fast neutrons, respectively. The gamma ray flux was  $1.25 \times 10^7 \text{ cm}^{-2}\text{s}^{-1}$ .

In the experiments for the present study, the MAGAT-type gel detector was infused with LiCl, where the naturally abundant isotope  $^6\text{Li}$  was used. The  $^6\text{Li}$  concentrations were set at 0, 10 and 100 ppm. The dimension of the gel detector was  $60 \times 60 \times 60 \text{ mm}^3$ . The gel detector was encased in a box made of 5 mm thick acrylic acid resin. The box was set inside a  $200 \times 200 \times 200 \text{ mm}^3$  acrylic acid resin phantom, to simulate a human head in a brain tumor treatment.

The response of the MAGAT to dose was measured. The irradiation was performed by using Co gamma rays irradiation facility at Hiroshima University. The transverse relaxation rate ( $R_2$ ) was determined using a 0.3T MRI scanner (AIRIS II comfort, Hitachi Medical Corp.) with a standards head coil.

The fluence  $\phi_j$  of each component was determined using the following model;

$$S = \begin{pmatrix} S_1 \\ S_2 \\ S_3 \end{pmatrix} = \begin{pmatrix} a_{11} & a_{12} & a_{13} \\ a_{21} & a_{22} & a_{22} \\ a_{31} & a_{32} & a_{33} \end{pmatrix} \begin{pmatrix} \Phi_1 \\ \Phi_2 \\ \Phi_3 \end{pmatrix} = A \cdot \Phi \quad (1),$$

$$\Phi = A^{-1} \cdot S \quad (2),$$

where  $a_{ij}$  denotes the sensitivity of the  $i$ th gel for the component  $j$ .

**RESULTS:** The raw signal intensity of the gel detector is shown in Figure 1(a). The data in Figure 1 (a) was corrected so that all the gel detectors would have the same dose-response as the gel detector without  $^6\text{Li}$ , and the background signal intensity was subtracted. The corrected result is shown in Figure 1 (b). The data at the depths of 2.5 and 57.5 mm, which are within the regions 0 to 5 mm away from the wall of the acrylic

acid resin box, were omitted from further analysis since the oxygen penetrating the wall reduced the polymerization and thus the signal intensity.

The results for the two-component estimation are shown in Figure 2. In this case, both the gamma rays and thermal neutrons are positive. The standard deviation is about 2% for gold activation, 10% for TLD, and 0.5% for the PHITS calculation. The fluence distribution measured by the gel detector agrees to within 20% to 30% of other estimates. This suggests the potential usability of polymer gel detector in spatial measurement of fluence in BNCT beam.

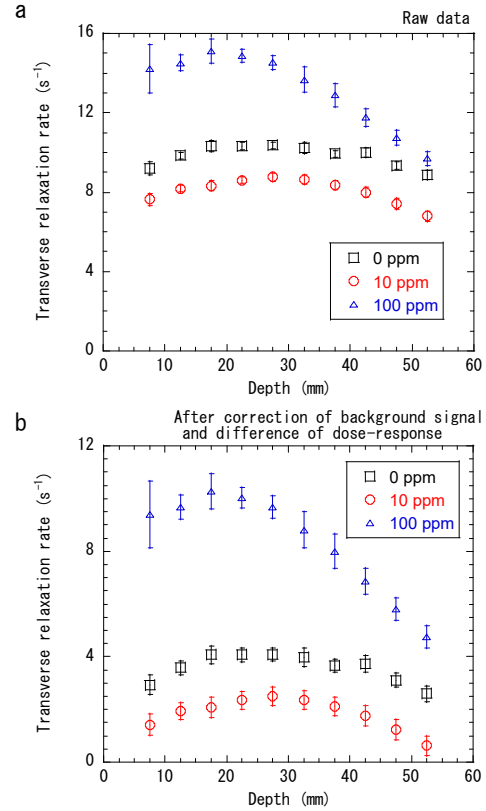


Fig. 1. Signal intensity ( $s^{-1}$ ), of the gel detector; (a) raw data, (b) after correction of background signal and difference of dose-response.

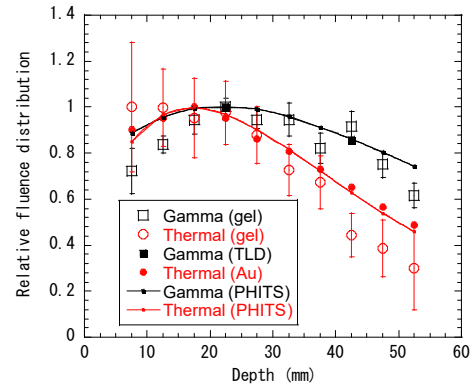


Fig. 2. Relative distribution of fluence estimated with two gel detectors with  $^6\text{Li}$  at 0 and 100 ppm.

K. Shinsho, R. Oh, M. Tanaka, S. Yanagisawa, H. Tanaka<sup>1</sup>, T. Takata<sup>1</sup>, G. Wakabayashi<sup>2</sup> and Y. Koba<sup>3</sup>

Graduate School of Human Health Science, Tokyo Metropolitan University

<sup>1</sup>Institute for Integrated Radiation and Nuclear Science, Kyoto University

<sup>2</sup>Graduate school of Science and Engineering Research, Kindai University

<sup>3</sup>Center for Radiation Protection Knowledge, QST-NIRS

**INTRODUCTION:** Boron Neutron Capture Therapy (BNCT) is one of the radiation therapies using neutrons and <sup>10</sup>B drugs which are attracted to tumors. BNCT is expected to be next-generation cancer therapy which will improve the QOL of patient because it is able to irradiate a cancer cell at the molecular level selectively. However, dosimetry techniques in mixed neutron-gamma fields have not been established yet. Therefore, we focused on reusable two-dimensional thermoluminescence dosimeter (2D-TLD). The 2D-TLD which we used is thermoluminescence (TL) phosphor Cr doped Al<sub>2</sub>O<sub>3</sub> ceramic plate (2-D Al<sub>2</sub>O<sub>3</sub>: Cr TLD).[1] 2-D Al<sub>2</sub>O<sub>3</sub>: Cr TLD that can acquire radiation images with high spatial resolution. In addition, it has high solidity and can be used under water. In this study, we investigated that neutron imaging using 2-D Al<sub>2</sub>O<sub>3</sub>: Cr TLD and Cd neutron-gamma ray converter technique in mixed neutron-gamma fields. The Cd neutron-gamma ray converter lets the sensitivity of the neutron increase selectively. As a result, we can acquire the neutron images easily without discrimination of gamma ray.

**EXPERIMENTS:** Low melting point Al<sub>2</sub>O<sub>3</sub> of Chibac ceramic MFG Co. LTD., which was composed of Al<sub>2</sub>O<sub>3</sub> > 99.5 wt% was used. The bulk density of the plates was 3.7g·cm<sup>-1</sup>. The dimensions used for the glow curve measurements were 10 × 10 × 0.7 mm<sup>3</sup>. The concentration of Cr<sub>2</sub>O<sub>3</sub> in the present study was 0.05 wt%. The assumed irradiation fields are the mixed neutron irradiation mode in KUR-HWNIF, with a power of 1MW. The glow curves were recorded from room temperature up to 400 °C at a heating rate of 0.1 °C·s<sup>-1</sup>. Fig.1 shows the Diagram of TLD irradiation arrangement for glow curve measurements. The Two - dimensional TL measurement system consists of a CMOS camera, 80 × 80 mm<sup>2</sup> heater, and a dark box. After exposure, the TL slabs were heated to 400 °C for 5 min. The TL images were captured using a CMOS camera equipped with a thermal cut filter.

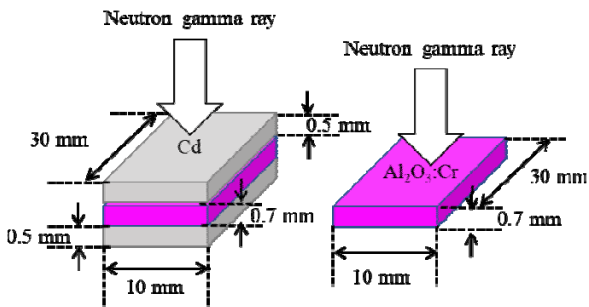


Fig.1. Diagram of TLD irradiation arrangement for glow curve measurements.

**RESULTS:** Figure2 shows the glow curve of Al<sub>2</sub>O<sub>3</sub>: Cr using Cd converter at mixed neutron irradiation mode in KUR-HWNIF. The glow peak of Al<sub>2</sub>O<sub>3</sub>: Cr was observed at 310 °C with and without Cd converter. In addition, the glow peak intensity was increased by installing the Cd converter. The TL sensitivity increased approximately 150 times using Cd converter. Table shows the relations between the thermal neutron fluencies and the γ- ray dose. The irradiation field contains gamma rays as well as neutrons, but the TL intensity of the TLD using the Cd converter is almost derived from neutrons.

Figure 3 shows the arrangement of TL slabs (Al<sub>2</sub>O<sub>3</sub>: Cr using Cd converter) irradiation arrangement for TL imaging and the TL image. We could take the thermal neutron image easily in the mixed neutron-gamma fields without to discriminate.

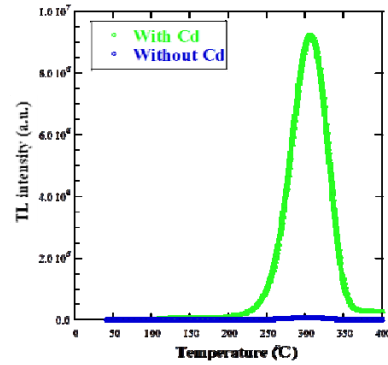


Fig.2. Glow curve of Al<sub>2</sub>O<sub>3</sub>: Cr using Cd converter at mixed neutron irradiation mode in KUR-HWNIF.

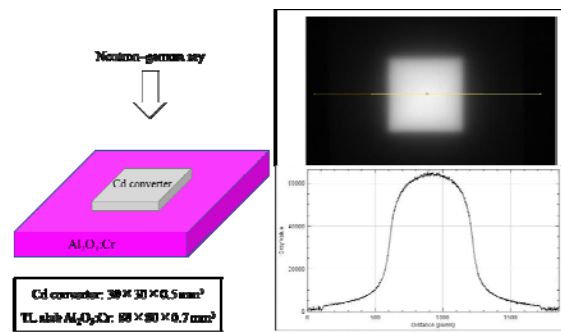


Fig.3. Left: Arrangement of TL slabs (Al<sub>2</sub>O<sub>3</sub>: Cr using Cd converter) irradiation arrangement for TL imaging. Right: TL image of the slab and the off axis ratio.

Table. Thermal neutron fluencies and γ- ray dose.

Thermal neutron fluencies[cm <sup>-2</sup> ]	Gamma-ray dose[Gy]
$7.2 \times 10^{15}$	0.61

**REFERENCES:** [1]K. Shinsho *et al.*, Sensors and Materials., **30** (2018) 1591-1.

## PR5-8 The Study for Development and Application of Tissue Equivalent Neutron Dosimeter

M. Oita, T. Kamomae<sup>1</sup>, T. Takata<sup>2</sup> and Y. Sakurai<sup>2</sup>

Graduate School of Interdisciplinary Science and Engineering in Health Systems, Okayama University

<sup>1</sup>Graduate School of Medicine, Department of Radiology, Nagoya University

<sup>2</sup>Institute for Integrated Radiation and Nuclear Science, Kyoto University

**INTRODUCTION:** Recent years, the clinical application of Accelerator-Based Boron Neutron Capture Therapy (AB-BNCT) has been introduced to make significant contributions to treatment for intractable cancer such as glioblastoma multiforme, superficial head and neck cancer, and melanoma in Japan.

In BNCT, the boron ( $n,\alpha$ )-reaction of the isotope  $^{10}\text{B}$  has a high cross-section toward thermal neutrons, and the produced alpha and lithium particles have a short-range on the micrometer scale. However, the neutron spectrum always spans a broad energy range, which results in different dose distribution and biological effects in tissue. A radiochromic film (RCF) is one of the most useful dosimetry tools in the advantages of high spatial resolution, small energy dependence, tissue equivalence, and self-development without processing in a darkroom<sup>1-3</sup>. The hydrogel material is also expected to use for a patient bolus in clinical radiotherapy<sup>4</sup>. In this work, the authors have developed new nanocomposite hydrogel for BNCT, which is highly expected to use for a patient bolus in clinical BNCT. Moreover, the hydrogel can improve dose distribution as well as can be manufactured arbitrary size and thickness using a 3D printer. Therefore, we have investigated to develop a system that enables dose optimization by optimally modulating the neutron beam for each patient using the hydrogel and RCFs.

**EXPERIMENTS:** Firstly, a reflective-type RCF, GAFCHROMIC® EBT3 (Ashland Inc., Wayne, NJ, USA) using a KUR neutron source was evaluated in this study. For irradiation,  $1.0 \times 1.0 \text{ cm}^2$  pieces of the RCF were placed at a depth of 0 cm to 24.2 cm in the air, water with 50ppm of boron, and water using the standard epithermal neutron irradiation mode of the Heavy Water Neutron Irradiation Facility at Kyoto University Research Reactor (KUR-HWNIF). Then, to assess the shielding effect of the 3D printed hydrogel for neutron beam, test slabs were fabricated. The thickness and clay nanoparticles concentration of the test slabs were varied from 2.5 to 5.2 wt%, respectively. The irradiation experiment was performed using KUR-HWNIF. Gold wires were used to estimate the neutron flux at the entrance and exit plane of the test slabs. Thermo-luminescent dosimeters

were used for the estimation of gamma-ray doses. The measured data were normalized by the values at the entrance plane of the test slabs.

**RESULTS:** Fig.1 shows the change of relative pixel values of RCFs irradiated by the KUR- HWNIF neutron source. Further analysis was needed for the response of RCFs with neutron components and contributions of gamma rays using Monte Carlo simulation and additional experiments with a cadmium filter. Fig. 2 shows a depth neutron flux and gamma-ray distribution with a change in the clay nanoparticles concentration (left: 2.6 wt%, right: 5.2 wt%). The results showed that the influence of NC gel was mainly the neutron thermalization (Epithermal neutrons loss their kinetic energy). The influence of the change in the clay nanoparticles concentration was almost unconfirmed. These phenomena would be affected by the buildup of neutron and gamma-ray doses. Our results demonstrated the feasibility of utilizing the 3D printed compensator to modulate the neutron beam intensity for clinical BNCT.

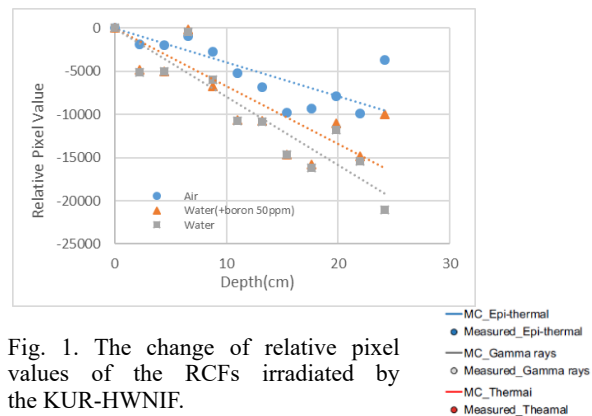


Fig. 1. The change of relative pixel values of the RCFs irradiated by the KUR-HWNIF.

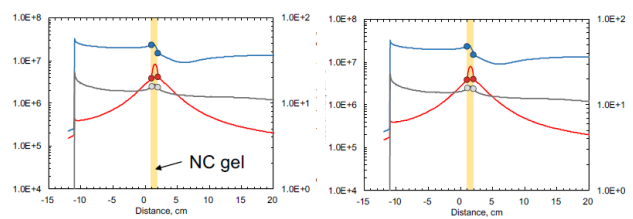


Fig. 2. Depth neutron flux and gamma-ray distribution with change in the clay nanoparticles concentration. (left: 2.6 wt%, right: 5.2 wt%)

### REFERENCES:

- [1] Niroomand-Rad, Azam *et al.*, Medical physics **25** (1998) 2093-2115.
- [2] Borca, Valeria Casanova *et al.*, Journal of applied clinical medical physics **14** (2013).
- [3] Fiandra, Christian *et al.*, Medical physics **40** (2013).
- [4] K Tanaka, Y Sakurai, *et al.* Applied Radiation and Isotopes **127** (2017) 253-259.

S. Hayashi, Y. Sakurai<sup>1</sup>, M. Suzuki<sup>1</sup>, and T. Takata<sup>1</sup>

Department of Clinical Radiology, Hiroshima International University

<sup>1</sup> Institute for Integrated Radiation and Nuclear Science, Kyoto University

**INTRODUCTION:** Three-dimensional (3D) gel dosimeters have been investigated for the 3D dose measurement of the complex conformal dose distributions in the clinical applications [1]. These devices utilize radiation-induced chemical reactions in the gel to preserve information about the radiation dose. The 3D absorbed dose distribution is deduced from the distribution of the reactant measured by imaging modalities, such as MRI, X-ray and optical computed tomography (CT). The applications to neutron irradiation have been also investigated, and the potential as a 3D dosimeter has been suggested [1].

Recently, we developed a novel radiochromic gel dosimeter that utilizes red color development due to the complexation of polyvinyl alcohol (PVA) with iodide ( $I_3^-$ ) formed in an aqueous solution by irradiation [2]. This gel dosimeter has excellent dose properties such as high sensitivity, dose rate independence, and a wide dose range, on X- and gamma-rays.

In this preliminary study, the optical-dose-response of the novel PVA-I (PVA-GTA-I) gel dosimeters [3] containing boron and lithium in the irradiation of neutron beams with different energy spectra from a nuclear reactor was examined and its availability was investigated.

**EXPERIMENTS:** As sensitizers, boric acid,  $B(OH)_3$ , containing  $^{10}B$  of 20% naturally, and lithium sulfate,  $Li_2SO_4$ , containing  $^6Li$  of 100% approximately, were added into the standard PVA-GTA-I gel, respectively. The concentrations in the gel were approximately 25, 50 mM of  $^{10}B(OH)_3$ , and 10, 20 mM of  $^6Li_2SO_4$ . The resulting solution was subdivided by pouring into PMMA cuvettes (4.5 mL, 1 cm path length).

The neutron irradiations were performed using Heavy Water Neutron Irradiation Facility (HWNIF) of Kyoto University Research Reactor (KUR, power of 1 MW). The samples were irradiated at 1, 2, 3, and 4 cm depths from surface in air at room temperature. The three different modes (thermal neutron rich for 30 min, epi-thermal and fast neutron rich for 50 min, and the mixed modes for 10 min) of neutron beams made by

heavy water spectrum shifter and cadmium thermal-neutron filters were applied to the samples.

The measurements were performed at room temperature using a UV-Vis spectrophotometer (SHIMADZU, UV-1600PC, Japan). The change in the absorbance ( $\Delta Abs.$ ) at the peak wavelength (486 nm) was investigated as the dose-response.

**RESULTS:** As examples, Figures 1(a) and 1(b) show that the depth-absorbance profiles obtained from our PVA-GTA-I gel dosimeters containing boron and lithium exposed to neutron beam of the epi-thermal and fast mode, respectively.

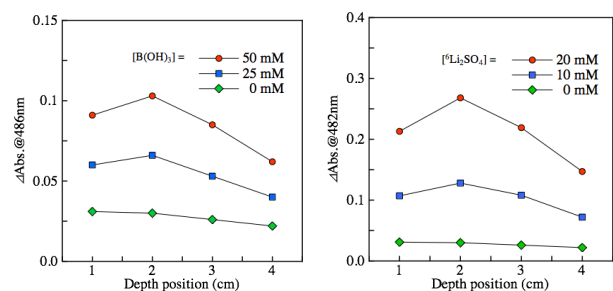


**Figure 1** Depth-absorbance distributions in epi-thermal and fast neutron mode of gel dosimeters with (a) boron and (b) lithium from the phantom surface.

The broad peaks were observed around 2 cm of depth in both dosimeters. The changes increased with the concentration of sensitizers. It is suggested that the peaks correspond to the distribution of the thermal neutron due to the moderation of epi-thermal neutron. It is noteworthy that the effect of lithium is larger than that boron in spite of the difference in their concentrations and absorption cross-sections. The effect was also observed in the other spectra modes.

These results suggest that both boron and lithium work as effective sensitizers on the thermal neutron in the PVA-I gel dosimeters.

#### REFERENCES:

- [1] C. Baldock *et al.*, *Phys. Med. Biol.* **55** (2010) R1–63.
- [2] S. Hayashi *et al.*, *Radiat. Meas.* **131** (2020) 106226.
- [3] J. E. Taño *et al.*, *Radiat. Meas.* (*in press*) (2020) 106311.

# PR5-10 Establishment of beam-quality estimation method in BNCT irradiation field using dual phantom technique (III)

Y. Sakurai, T. Takata, H. Tanaka, N. Kondo, M. Suzuki

*Institute for Integrated Radiation and Nuclear Science,  
Kyoto University*

**INTRODUCTION:** Research and development into several types of accelerator-based irradiation systems for boron neutron capture therapy (BNCT) is underway [1,2]. Many of these systems are nearing or have started clinical trials. Before the start of treatment with BNCT, the relative biological effectiveness (RBE) for the fast neutrons (over 10 keV) incident to the irradiation field must be estimated.

Measurements of RBE are typically performed by biological experiments with a phantom. Although the dose deposition due to secondary gamma rays is dominant, the relative contributions of thermal neutrons and fast neutrons are virtually equivalent under typical irradiation conditions in a water and/or acrylic phantom. Uniform contributions to the dose deposited from thermal and fast neutrons is based in part on relatively inaccurate dose information for fast neutrons.

The aim of this study is the establishment of accurate beam-quality estimation method mainly for fast neutrons by using two phantoms made of different materials, in which the dose components can be separated according to differences in the interaction cross-sections. The fundamental study of a “dual phantom technique” for measuring the fast neutron component of dose is reported [3].

In 2019, verification experiments for the dual phantom technique were performed using Heavy Water Neutron Irradiation Facility installed in Kyoto University Reactor (KUR-HWNIF). Biological experiments were performed using the solid phantoms, which were made based on the simulation results in 2018.

**METHODS:** One of the dual solid phantoms was made of polyethylene with natural lithium fluoride for 30 weight percent (LiF-polyethylene phantom), and the other phantom was made of polyethylene with 95%-enriched lithium-6 fluoride for 30 weight percent (<sup>6</sup>LiF-polyethylene phantom).

Vials containing one kind of human brain cell, such as U87ΔEGFR, were placed at the surface, 2-cm depth, 5-cm depth and 8-cm depth in the phantoms on the center axis of the beam line. Cell growth assay was performed for the irradiated cells.

The neutron flux and gamma-ray dose rate along the central axis in the phantoms were measured using activation foils and thermo-luminescent dosimeter, respectively. The depth dose distributions for the thermal neutron, fast neutron and gamma-ray components were determined based on the simulation calculation results normalized referring to the measured values.

Figure 1 shows a schematic of the experimental setup.

**RESULTS:** Figures 2 and 3 show the depth distributions for the thermal neutron dose, fast neutron dose, gamma-ray dose, and total dose in the LiF-polyethylene phantom and the <sup>6</sup>LiF-polyethylene phantom, respectively. It was confirmed that the dose contribution of fast neutrons is improved from approximately 10% in the LiF-polyethylene phantom, to approximately 50% in the <sup>6</sup>LiF-polyethylene phantom.

**CONCLUSION:** The assay results are presently being analyzed in association with the data of the depth dose distribution for the thermal neutrons, fast neutrons and gamma-rays. The biological experiments using the other cell lines are under planning.

**ACKNOWLEDGMENT:** This work was supported by JSPS KAKENHI Grant Number JP 16H05237.

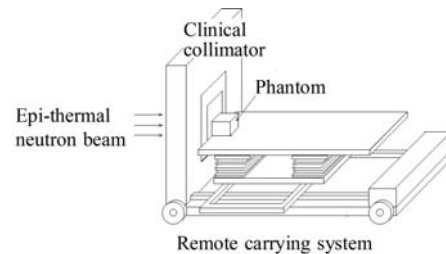


Fig. 1. A schematic of the experimental setup.

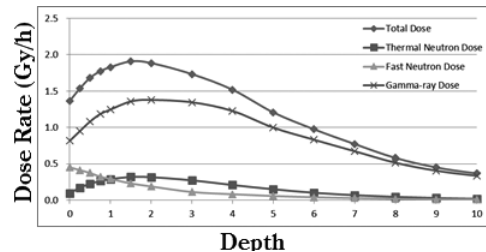


Fig. 2. Depth dose distributions in the LiF-poly phantom.

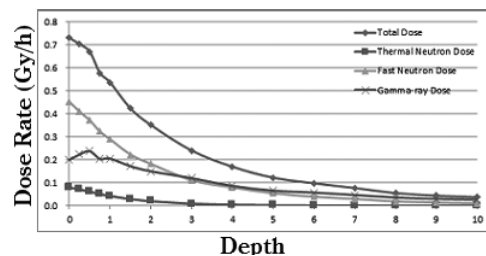


Fig. 3. Depth dose distributions in the <sup>6</sup>LiF-poly phantom.

## REFERENCES:

- [1] H. Tanaka *et al.*, Nucl. Instr. Meth. B **267** (2009) 1970-1977.
- [2] H. Kumada *et al.*, Appl. Radiat. Isot. **88** (2014) 211-215.
- [3] Y. Sakurai *et al.*, Med. Phys. **42** (2015) 6651-6657.

## PR5-11 Characteristics test of a Prompt Gamma-ray detector using LaBr<sub>3</sub>(Ce) Scintillator and 8 x 8 Array MPPC for Boron Neutron Capture Therapy

K. Okazaki, K. Akabori<sup>1</sup>, T. Takata<sup>2</sup>, S. Kawabata<sup>3</sup>, Y. Sakurai<sup>2</sup>, H. Tanaka<sup>2</sup>

Graduate School of Engineering, Kyoto University

<sup>1</sup>Sumitomo Heavy Industries

<sup>2</sup>Institute for Radiation and Nuclear Science, Kyoto University

<sup>3</sup>Osaka Medical College

**INTRODUCTION:** Boron neutron capture therapy (BNCT) is employed to treat cancer cells using a <sup>10</sup>B compound and a neutron beam. Basically, the range of the heavy particles, which are produced by the (n,  $\alpha$ ) reaction between <sup>10</sup>B and thermal neutrons, is shorter than the diameter of a cell. A <sup>10</sup>B compound accumulates <sup>10</sup>B into tumor cells, and into normal cells slightly. To determine the prescript dose during the treatment, it is necessary to measure the <sup>10</sup>B concentration in tumor and normal tissue in real-time. At present, it is obtained using a high purity germanium detector with prompt gamma-ray analysis at the Institute for Integrated of Radiation and Nuclear Science, Kyoto University Integrated for Radiation and Nuclear Science (KURNS)[1,2]. However, this method is not able to attain the <sup>10</sup>B concentration during the irradiation. Thus, a prompt gamma-ray imaging detector system has been developed. It consists of a LaBr<sub>3</sub>(Ce) scintillator and an 8 x 8 channel multi-pixel photon counter (MPPC), 64 channels amplifiers, a shaper and analog-to-digital converters (ADCs). This paper reports the concept underlying this system and the results of characterizing this system.

**EXPERIMENTS:** The size of the LaBr<sub>3</sub>(Ce) scintillator was 50 mm x 50 mm x 10 mm[3]. The scintillator was put in front of an 8 x 8 array MPPC. An MPPC is a type of silicon photomultiplier, and the effective active area of one channel of an MPPC is 6 x 6 mm<sup>2</sup>. The outputs of 64 channels were fed to an amplifier unit. The 64 analog outputs were digitalized by ADCs. These digital signals were stored in a PC. Firstly, gain in each channel of the MPPC was adjusted. Secondly, gamma ray spectra from an Na-22 source, which emitted 511 keV gamma rays, were attained in order to confirm that the energy resolution at 511 keV. Finally, gamma ray spectra using samples with 25 and 50 ppm were obtained by irradiating thermal neutrons at the Kyoto University Reactor neutron guide tube. To discriminate between 478 keV and 511 keV gamma rays, the Gaussian distribution for the two gamma rays was defined.

**RESULTS:** The average energy resolution of this detector system at 511 keV gamma rays was approximately 5.0 $\pm$ 0.2 %. Fig.1 shows the spectrum at the center channel of the MPPC obtained with 25 ppm and the region of interest (ROI) in the Gaussian distribution for 478 keV gamma rays set up as  $-3\sigma$  to the median. In addition, the count rate of 478 keV gamma rays with 25 and 50 ppm samples were calculated in the ROI. Moreover, gamma

ray peak at 511 keV did not overlap 478 keV peak so much. The count rate of 478 keV gamma rays with 25 ppm sample in the ROI was 0.23 that was sufficient to obtain counts to be below 10 % statistic error within an hour. In addition, the linearity of the count rate at 478 keV gamma rays and <sup>10</sup>B concentration was confirmed as shown as Fig. 2.

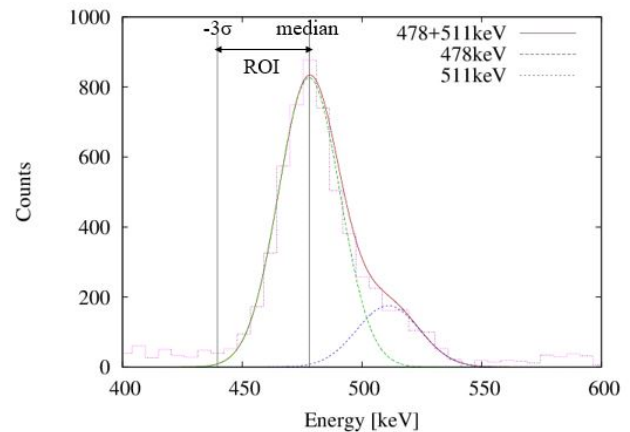


Fig. 1. Gamma rays spectrum at the center channel with 25 ppm.

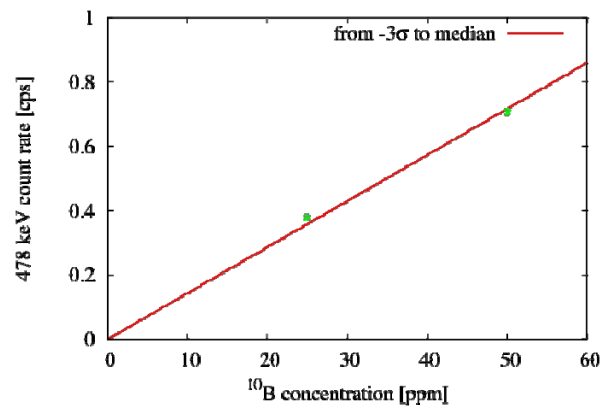


Fig. 2. The linearity between <sup>10</sup>B concentration and 478 keV count rate.

### REFERENCES:

- [1] T. Kobayashi and K. Kanda, Nucl. Instruments Methods Phys. Res., vol. 204, pp. 525-531, 1983.
- [2] J. Laakso, M. Kulvik, I. Ruokonen, and J. Va, Clin. Chem, vol 47, No. 10, pp. 1796-1803, 2001.
- [3] E. V. D. van Loef, P. Dorenbos, C. W. E. van Eijk, K. Krämer, and H. U. Güdel, Appl. Phys. Lett., vol. 1573, pp. 1-4, 2013.

S. Kurosawa<sup>1,2</sup>, S. Kodama<sup>2</sup>, T. Takada<sup>3</sup>, Y. Sakurai<sup>3</sup>, H. Tanaka<sup>3</sup>

<sup>1</sup>New Industry Creation Hatchery Center, Tohoku University

<sup>2</sup>Institute for Materials Research Tohoku University

<sup>3</sup>Institute for Integrated Radiation and Nuclear Science, Kyoto University

**INTRODUCTION:** In the extremely high radiation dose condition such as inside of nuclear powerplant after the accident (decommissioning), a real-time-remote radiation-monitor is required to survey the internal condition. To avoid the radiation damage of the detectors or circuits, the use of a long silica optical fiber (over ~100-m-length) is proposed to read scintillation photons from the high dose condition [1] as shown in Fig. 1. To detect the scintillation photons efficiently through such a long optical fiber, high-light output and red- or NIR-emitting scintillators are suitable than blue or yellow photons to suppress the transmission loss.

We suggest to apply our developed red-emitting scintillator  $\text{Cs}_2\text{HfI}_6$  (CHI) to the fiber-read radiation monitor for the decommissioning. CHI has a broad scintillation emission from 500 nm up to 800 nm with a peak at around 700 nm, a short decay time of  $\sim 1.9 \mu\text{s}$  among the red-phosphors and high light output of 64,000 photons/MeV [2]. In this study, we demonstrated such fiber-reading systems under the high-dose condition at the  $^{60}\text{Co}$  Gamma-ray Irradiation Facility in Institute for Integrated Radiation and Nuclear Science, Kyoto University.

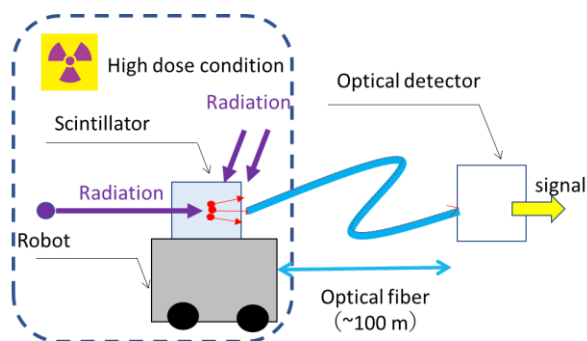


Fig. 1. Schematic view of real-time dose monitor.

**EXPERIMENTS:** We prepared a small CHI piece with a size of 2 mm x 3 mm x 1 mm by Bridgeman method. Due to hygroscopic nature, CHI was embedded in the optical cement (BC-600, Saint-Gobain Crystal) with a size of 3 mm x 4 mm x 1.5 mm. The CHI-cement sample was irradiated with gamma-rays from a  $^{60}\text{Co}$  source with an activity of  $\sim 100 \text{ TBq}$ , and the gamma-ray air dose rates at certain points on the experimental apparatus were estimated by Sato et al. [3]. Also, we fabricated Cr-doped  $\alpha\text{-Al}_2\text{O}_3$  sample (Ruby) with the same size and shape including the cement as that of CHI to compare the scin-

tillation photons.

The CHI and ruby-cement specimens were put on the tip of an optical fiber (S.600/600B, Fujikura) with a length of 20 m and pure  $\text{SiO}_2$  core diameter of  $600 \pm 30 \mu\text{m}$ . The scintillation light was transmitted through the fiber and measured with a CCD spectrometer (Blue-UVNb, StellarNet). We determined the scintillation signal intensity from the emission spectrum: integration of the emission area. The exposure time of the CCD camera was 5 sec for one time, and the measurements were repeated three times for each dose rate position.

**RESULTS:** We succeeded in observation of emission for CHI and also ruby with monitorable dynamic range of  $10^{-2}$  up to 1 kSv/h for the first time, and emission intensities as a function of the dose rate are displayed in Fig. 2. The data was linear-fitted by  $I = ax + b$ , where  $I$  and  $x$  are the intensity and the dose rate, respectively, and coefficients ( $a$ ,  $b$ ) is  $(9.4 \times 10^5, 3 \times 10^3)$  and  $(1.4 \times 10^5, 3 \times 10^3)$  for CHI and ruby, respectively.

The transition loss through the optical fiber for CHI was larger than that of ruby due to slightly shorter emission peak; nevertheless, the scintillation signal of emission integrated area of CHI was the highest due to the high light output. Combining with the quick response against gamma-rays with no afterglow, we should obtain a more accurate and reliable signal when CHI is used as a scintillation probe than ruby. The detail of this collaboration study is described in [4].

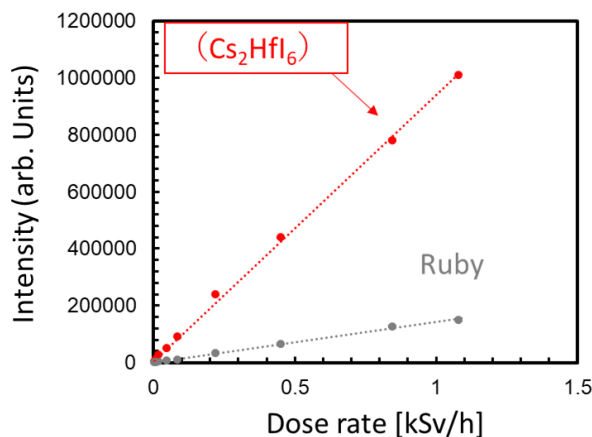


Fig. 2. Emission intensities for CHI and ruby excited by gamma rays ( $^{60}\text{Co}$ ) as a function of the dose rate.

#### REFERENCES:

- [1] C. Ito, *et al.*, J. Nucl. Sci. Technol. **51** (2014) 944.
- [2] S. Kodama, S. Kurosawa *et al.*, Radiat. Meas. **124**, (2019) 54.
- [3] N. Sato *et al.*, (2008). at <http://www.rri.kyoto-u.ac.jp/gamma/doseratesheet.pdf>
- [4] S. Kodama, S. Kurosawa and H. Tanaka *et al.*, Applied Physics Express **13**, (2020) 047002.

# PR5-13 Establishment of the Imaging Technology of 478 keV Prompt Gamma-rays of Boron-neutron Capture Reaction and the Measurement of the Intensity of the Neutron Field

T. Mizumoto, S. Komura, Y. Sakurai<sup>1</sup>, A. Takada<sup>2</sup>,  
T. Takata<sup>1</sup>, T. Tanimori<sup>2</sup>

Fukushima SiC Applied Engineering Inc.

<sup>1</sup>KURNS

<sup>2</sup>Graduate School of Science, Kyoto University

**INTRODUCTION:** BNCT is one of the promising cancer treatment methods. However, we have not yet obtained a good monitoring method of the treatment effect in real-time during BNCT. The main reason is that it is difficult to know precisely both the boron concentration and neutron flux intensity in tumor cells and healthy ones. If we get images of 478 keV gamma-rays generated by the boron-neutron capture reaction, and measure their intensity and generation positions, we can check the treatment effect on BNCT. To get gamma-ray images, several detectors such as SPECT and Compton cameras have been proposed. However, they have not been established due to their weaknesses [1]. To overcome the current situation, we have been developing electron tracking Compton cameras (ETCCs) which can uniquely determine the arrival direction of sub-MeV/MeV gamma ray event by event. An ETCC is the complex detector of two sub detectors: a time projection chamber TPC (Compton scatterer and recoil electron detector) and a scintillation camera (scattering gamma-ray absorber)[2][3].

**EXPERIMENTS:** We developed an ETCC which has a scintillation camera constructed with 576 pixelated GSO scintillators, whose pixel size is 6 mm×6 mm (26 mm in high), and a TPC whose size is 330 cm<sup>2</sup> (20 cm in high). As the performance measurement of the ETCC, we carried out two types of measurements at the Institute for Integrated Radiation and Nuclear Science, Kyoto University (KURNS). The first type was performed with E3 neutron guide tube of Kyoto University Reactor (KUR) (1 MW). We irradiated a Boron target (high concentration Boron solution) with a thermal neutron beam from E3 tube. We set the ETCC near the target and measured gamma rays from the target. The exposure time was a few hours. Another type of measurement was performed at KUR heavy water neutron irradiation facility. We set a (20 cm)<sup>3</sup> Boron solution target in the irradiation room, and the ETCC on the ceiling of the room. We set both the target and the ETCC on the axis of the cylindrical hole about 11 cm in diameter in the ceiling. We also set a LiF-containing Teflon plate between the ETCC and the hole as the shielding of thermal neutrons.

**RESULTS:** Fig. 1 shows the photograph and meas-

urement results with E3 tube. Measurement was performed for two target positions. From the result, we can see a clear positional difference between the two 478 keV gamma-ray images. We confirm 478 keV clear peak in spectra. Fig. 2 shows the schematic, photograph and measurement results with Heavy Water Neutron Irradiation Facility (epithermal neutron irradiation mode). The gamma-ray flux is approximately 10<sup>3</sup> /cm<sup>2</sup>/sec in front of the ETCC. Despite such the intense gamma-ray radiation environment, where the conventional Compton cameras are disturbed by random coincidence noise, our ETCC succeeded to detect the 478 keV prompt gamma rays arrived from the water phantom target as we can see in the spectra (a) and (b). In the prospects, we also need to try the measurement test in the high neutron flux condition.

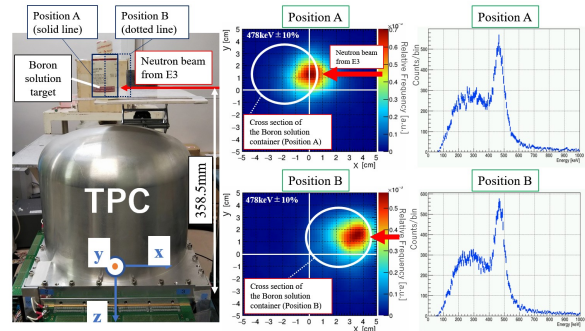


**Fig.1. Photo and results of the experiment with E3 tube. Left: photo taken on the measurement. Right: back-projection 478 keV gamma-ray images using the ML-EM method and spectra taken by the ETCC. Measurement was performed for two target positions. The positional difference between A and B is 4 cm.**

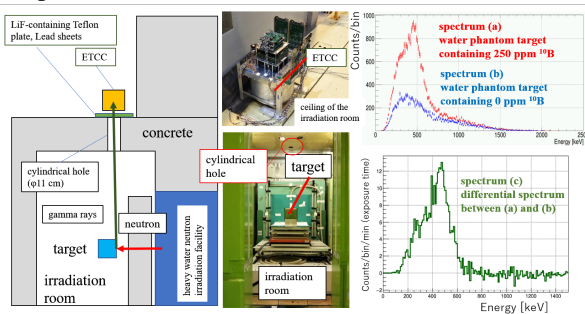


**Fig.2. Schematic view, photograph and gamma-ray energy spectra of the experiment with heavy water neutron irradiation facility. ETCC measured gamma-rays from the treatment room. <sup>10</sup>B concentration of water phantom target is 250 ppm and 0 ppm.**

**REFERENCES:**

- [1] T. Mizumoto, KURNS Progress Report 2018 (2019).
- [2] Y. Mizumura, JINST, 9, (2014) C05045.
- [3] T. Mizumoto, JINST 10 (2015) C06003.

## PR5-14 Feasibility study of a gel-dosimeter for a quality assurance and a quality control in boron neutron capture therapy

S. Nakamura<sup>1,2</sup>, K. Iijima<sup>1</sup>, M. Takemori, H<sup>1</sup>. Nakayama<sup>1</sup>, S. Nishioka<sup>1,2</sup>, H. Okamoto<sup>1,2</sup>, Y. Sakurai<sup>3</sup>, H. Tanaka<sup>3</sup>, N. T. Takata<sup>3</sup>, M. Suzuki<sup>3</sup>, H. Igaki<sup>2,4</sup>, and J. Itami<sup>2,4</sup>

<sup>1</sup>Department of Medical Physics, National Cancer Center Hospital

<sup>2</sup>Division of Research and Development for Boron Neutron Capture Therapy, National Cancer Center Exploratory Oncology Research & Clinical Trial Center

<sup>3</sup>Institute for Integrated Radiation and Nuclear Science, Kyoto University

<sup>4</sup>Department of Radiation Oncology, National Cancer Center Hospital

**INTRODUCTION:** In boron neutron capture therapy (BNCT), the neutron irradiation to the patient is performed after a sufficient accumulation of  $^{10}\text{B}$  to tumor cells because the treatment efficacy is based on the  $^{10}\text{B}(n,\alpha)^7\text{Li}$  reaction. It is important for the radiation therapy that the delivered dose is verified as a quality assurance before the treatment. However, it is a difficult for the existing detector that the three dimensional dose distribution is measured in BNCT with considering a non-uniformity of  $^{10}\text{B}$  on the actual patient. Thus, this study focuses on the gel-dosimeter for the three dimensional dosimetry in BNCT. There are some reasons. First, the gel-dosimeter can mix a few  $^{10}\text{B}$  with keeping the dose response. Second, the gel-dosimeter is generally used for the three dimensional dosimeter. Third, the gel-dosimeter is not expensive, and the quality assurance using the gel-dosimeter may not affect the medical costs in BNCT. Therefore, this study aims to evaluate the dose response dependence of the gel-dosimeter which contains a certain boron-10 density in BNCT.

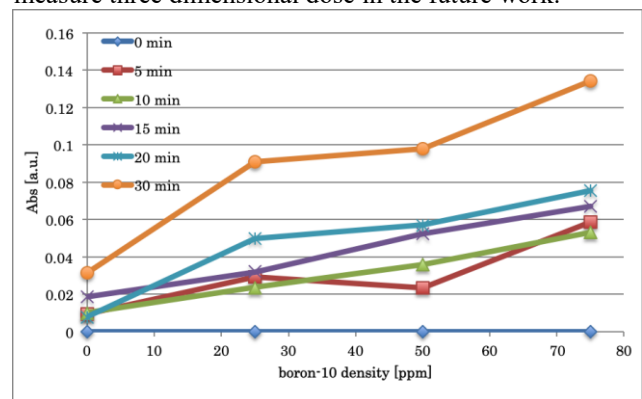
**EXPERIMENTS:** The experiment was performed in the Heavy Water Neutron Irradiation Facility (Kyoto University Reactor, KUR). The KUR was operated at a power of 1 MW. The neutrons were delivered to the gel-dosimeter which composed of water, PVA, KI, KCl, Gellan gum, Fructose, and boron solutions. The boron-10 density of the gel-dosimeter was 0, 25, 50, and 75 ppm. The irradiation time was set to 0, 5, 10, 15, 20, 30 min in each gel-dosimeter. After the neutron irradiation, the dose response in each gel-dosimeter was read by an optical scanner. The dose response dependence in each gel-dosimeter was evaluated.

**RESULTS:** Figure 1 (a) shows the dose responses of gel-dosimeter in each boron-10 density and (b) shows those in each irradiation time. According to Fig.1, the dose response increases with boron-10 density and irradiation time. Figure 2 shows the difference of dose response among the irradiation positions on the beam port. The dose response of gel-dosimeter positioned at the center on the beam port was higher than that positioned at the edge.

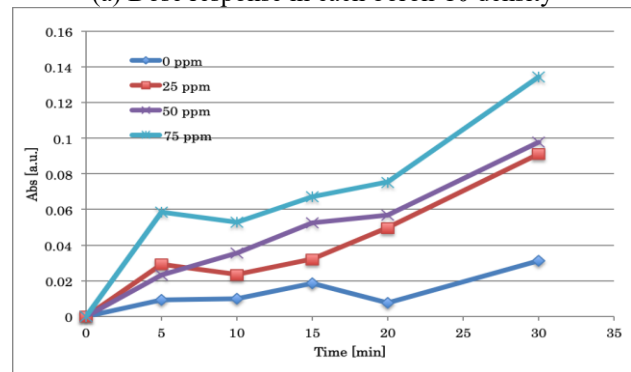
**Discussion:** This study suggests that the gel-dosimeter has a sufficient sensitivity for the reaction

of  $^{10}\text{B}(n,\alpha)^7\text{Li}$  in BNCT although the boron-10 density expects very low (25 ppm, etc...). According to fig. 1, the dose response in the gel-dosimeter increases with the boron-10 density and the irradiation time, and it seems that the dose response can evaluate the actual dose delivered to the gel-dosimeter (Fig. 2). On the other hand, linearity of the dose response against the boron-10 density is not sufficient. It may relate to a creating method of the gel-dosimeter. Some different method will be tried to seek the best method for creating the gel-dosimeter in the future work.

**Conclusion:** We performed the feasibility test of the gel-dosimeter whether it could evaluate the three dimensional dose distribution in BNCT. The possibility for the evaluation could be indicated in this study. We will try to measure three dimensional dose in the future work.



(a) Dose response in each boron-10 density



(b) Dose response in each irradiation time

Fig. 1. Dose response of gel dosimeter.

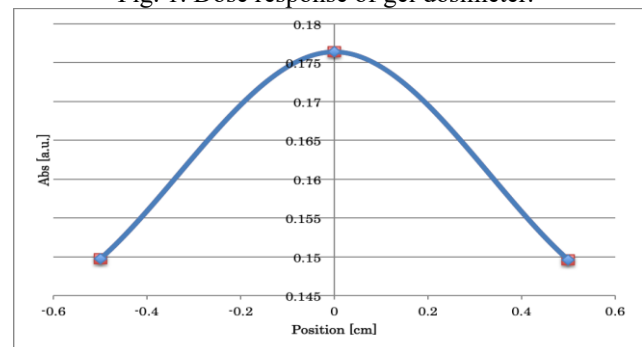


Fig.2. Dependence of position.

T. Takata, H. Tanaka, A. Sasaki<sup>1</sup>, Y. Sakurai, A. Maruhashi and M. Suzuki

*Institute for Integrated Radiation and Nuclear Science, Kyoto University*

<sup>1</sup>*Graduate School of Engineering, Kyoto University*

**INTRODUCTION:** In Boron Neutron Capture Therapy (BNCT), epithermal neutron beam has been utilized to treat a deep-seated tumor due to its high penetration ability based on thermalization within a patient. However, thermal neutron buildup causes dose deficiency in a case for a tumor locating in a vicinity of a patient surface. In such a case, a bolus consisting of a hydrogen-rich material has been utilized to improve the dose distribution. In present clinical BNCT, a bolus with a uniform thickness and a simple shape has been adopted. Aiming to more aggressively increase tumor dose, an optimizing method of bolus shape was studied.

**MATERIALS AND METHODS:** The optimization was performed as following. At first, a beam incident direction was determined according to location of a planning target volume (PTV) and organs at risk (OARs). Then, control points to define bolus thicknesses were assigned on the beam incident surface. A bolus region was modeled in a patient geometry by interpolating the thicknesses defined at the control points. These procedures were illustrated in Fig. 1. The thicknesses at the control points were adjusted to maximize a PTV dose under OAR dose regulations through an optimization calculation. As an example, a case for parotid cancer extended into a subcutaneous region was examined.

*Patient geometry modelling:* A PTV around a parotid gland and an OAR for an oral mucosa were delineated on X-ray CT images of a head phantom by a radiation oncologist. Then, a patient geometry model was constructed for radiation transport calculations. A beam direction was determined so that the PTV was centered in an irradiation field while locating the OAR in a deeper side.

*Bolus formation:* A bolus forming area was limited within a surface area in a 5-cm distance from the beam incident point. Control points were assigned to voxels in the area by using a  $1.5 \times 1.5 \times 1.5 \text{ cm}^3$  mesh-grid down sampling method. A bolus region was generated in the patient geometry by using an inverse-distance weighted interpolation of the thicknesses of the control points.

*Neutron and photon transport calculation:* The transport calculations were performed by using a Monte Carlo transport calculation module implemented in SERA; the treatment planning system for BNCT [1]. An epithermal neutron beam of the KUR heavy water neutron irradiation facility with an aperture diameter of 12 cm was assumed in the calculations [2]. The results were analyzed by using a dose evaluation module of SERA.

*Optimization calculation:* The maximum dose of the

oral mucosa was fixed to be 12 Gy-Eq according to the treatment protocol of BNCT for a head and neck cancer performed at KUR. Under this condition, an objective function was defined as the minimum dose of the PTV. The bolus thicknesses were adjusted to maximize the objective function by using a steepest gradient descent method.

**RESULTS:** The location of the PTV and OAR is shown in Fig. 2. The control points were assigned to 43 surface voxels by using the method described above. The iterative calculation was started from bolus thicknesses of zero at all control points. The result is shown in Fig. 3, where increase and convergence in the PTV dose according to iteration are confirmed. Fig. 2 also shows the resulting bolus shape at the 5<sup>th</sup> iteration, at which the objective function is almost converged. The growth of the bolus was observed around the area under which the PTV was extended into the subcutaneous region.

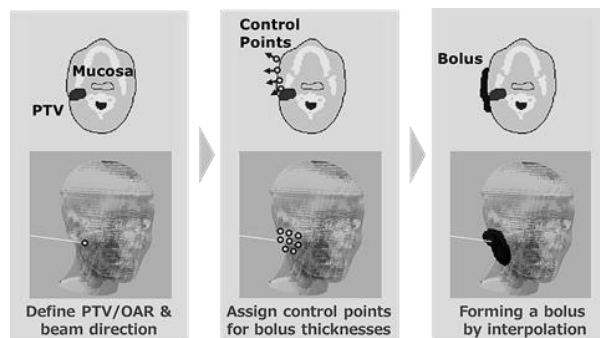


Fig. 1. Procedure of bolus formation.

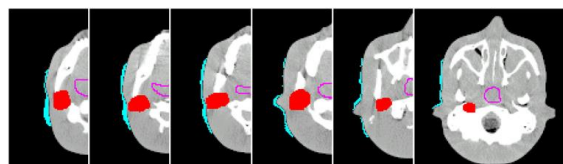


Fig. 2. Patient geometry with an optimized bolus.

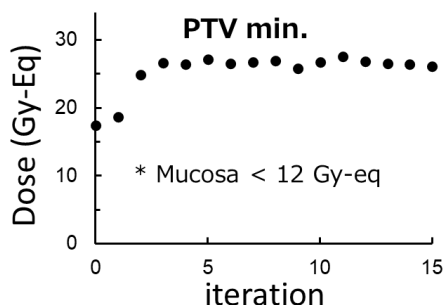


Fig. 3. Change in the objective function according to an iterative calculation.

### REFERENCES:

- [1] D. E. Wessol *et al.*, INEEL/EXT-02-00698 (2002).
- [2] Y. Sakurai, T. Kobayashi, *Med. Phys.* **29** (2002), 2328-2337.

H. Yasuda<sup>1</sup>, JE. Tano<sup>1,2,3</sup>, CAB. Gonzales<sup>1</sup>, Y. Sakurai<sup>4</sup>

<sup>1</sup>Department of Radiation Biophysics, RIRBM, Hiroshima University

<sup>2</sup>Graduate School of Biomedical and Health Sciences, Hiroshima University

<sup>3</sup>Phoenix Leader Education Program for Renaissance from Radiation Disaster, Hiroshima University

<sup>4</sup>Institute for Integrated Radiation and Nuclear Science, Kyoto University (KURNS)

**INTRODUCTION:** The flexibility of a gel dosimeter offers the advantage of providing 3D dose distribution in brain formed with complex geometries in the boron neutron capture therapy (BNCT) which is a chemically targeted treatment based on the nuclear reaction  $^{10}\text{B}(n,\alpha)^7\text{Li}$ . The authors have investigated application of a novel radiochromic gel made of polyvinyl alcohol (PVA), glutaraldehyde (GTA), and iodide (I) using gamma rays [1,2]. The present study explores the feasibility of the PVA-GTA-I gels infused with boric acid by evaluating their dose responses and sensitivities to epithermal neutron beams that are used for brain tumor treatment.

**EXPERIMENTS:** The gel samples were produced using analytical grade from Fujifilm Wako Pure Chemical Co., Japan and prepared one day before irradiation. The formula of each sample set is summarized in Table 1. Boric acid contains approximately 20% of  $^{10}\text{B}$  which equates to ~50 ppm and 200 ppm for 25 and 100 mM, respectively. The solution was poured into PMMA cuvettes and stored inside a vacuum chamber (-0.08 MPa) for 1-hour to remove the dissolved oxygen. Then, the samples are covered with lids and placed inside an oven at 45°C for 12 hours to allow gelation.

The neutron irradiation of the gel samples was carried out at the Heavy Water Neutron Irradiation Facility of Institute (HWNIF) for Integrated Radiation and Nuclear Science, Kyoto University with a nominal power of 1MW. The samples were fixed on an acrylic plate such that the axes of the cuvettes are perpendicular to the source and irradiated at different periods: 15, 30, and 60 min. Optical absorbance of the gel was measured with a UV-Vis spectrometer (Thermo Fisher Scientific Inc., USA).

Table 1. Compositions of PVA-GTA-I gels infused with different boric acid concentrations

Reagent	Concentration
Polyvinyl alcohol (PVA)	10 wt%
Ultrapure water	90 wt%
Glutaraldehyde (GTA)	0.01 M
Potassium Iodide (KI)	0.1 M
Glucono- $\delta$ -lactone (GDL)	0.1 M
Fructose	0.1 M
Boric acid	0, 25, and 100 mM

**RESULTS:** As shown in Fig. 1, optical absorbance of the PVA-GTA-I gels with higher boron concentration increased significantly after neutron exposure. Moreover, all the samples exhibited good dose-response linearities despite the low sensitivity from the standard formula of the PVA-GTA-I gel (i.e, without boric acid). This is further visualized in Fig. 2 wherein an increasing color intensity gradient is seen from the samples with 100 mM of boric acid.

These data indicate the feasibility of the boron-infused PVA-GTA-I gel for 3D dose assessment in BNCT. In addition, the results implied that the potential of combination of two or three PVA-GTA-I gels having different boron concentrations could enable us to distinguish the doses from neutrons and gamma rays. Further investigations are now under way.

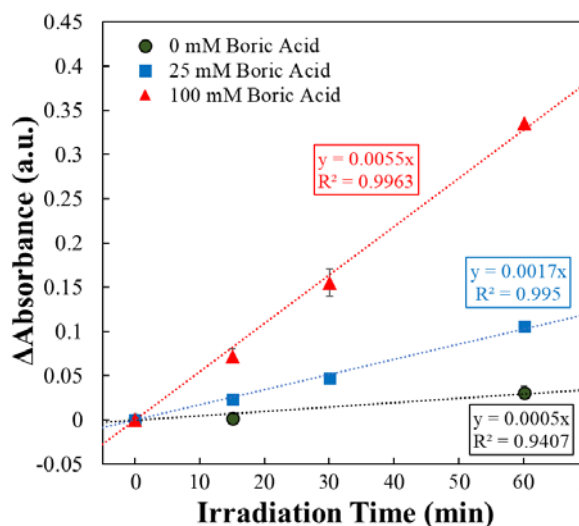


Fig. 1. Increments of the optical absorbances of the PVA-GTA-I gels infused with different-level boric acid concentrations as a function of irradiation time. Each data set is fitted with a linear function curve.



Fig. 2. A photo image of the PVA-GTA-I gel with 100 mM boric acid at 15, 30, and 60 min after neutron irradiation.

#### REFERENCES:

- [1] Taño JE *et al.*, 2019. *J Phys Conf Ser.*, **1305** 012034.
- [2] Taño JE *et al.*, 2020. *Radiat Meas* 106311.

## PR5-17 Measurement of neutron distributions in the BNCT irradiation field using a GEM detector

S. Uno, T. Koike<sup>1</sup>, K. Miyamoto<sup>2</sup>, K. Nobori<sup>2</sup>, H. Tanaka<sup>3</sup>

High Energy Accelerator Research Organization (KEK)

<sup>1</sup> Faculty of Health Sciences, Kyorin University

<sup>2</sup> BeeBeans Technologies Co.Ltd

<sup>3</sup> Institute for Integrated Radiation and Nuclear Science, Kyoto University

**INTRODUCTION:** The boron neutron capture therapy (BNCT) is a radiation therapy to destroy tumor cells selectively based on a nuclear reaction when  $^{10}\text{B}$  is irradiated with thermal neutrons. Epithermal neutrons are suitable for the BNCT, because thermal neutrons are effectively irradiated on tumor cells after epithermal neutrons are moderated in the tissue. Therefore, it is important to know the spatial distribution of epithermal neutrons in the treatment planning. For a measurement of the spatial distribution in thermal and epithermal neutrons irradiation field in the BNCT, we have been developing a two-dimensional real time imaging detector with the gas electron multiplier (GEM) [1]. The GEM is a position-sensitive device with the gas amplification to detect charged particles, photons, and neutrons. In this study, the performance of the GEM detector was evaluated using the Heavy Water Neutron Irradiation Facility (HWNIF) of the Kyoto University Research Reactor (KUR) [2].

**EXPERIMENTS:** Our GEM detector has a compact body with dimensions, 444 mm  $\times$  270 mm  $\times$  41 mm. It consists of a GEM chamber and a readout electronics board [3]. The effective detection area is 100 mm  $\times$  100 mm. The ASIC for the amplification and the FPGA for the online processing are mounted on the electronics board, which is able to transfer data directly to a PC via the net-work. Fig. 1 shows a schematic cross-section of the GEM chamber with a  $^{10}\text{B}$ -coated cathode plate. The detector works as a gas radiation detector for neutrons by detecting the charged particles emitted through a  $^{10}\text{B}(n, \alpha)^7\text{Li}$  nuclear reaction. Ionization electrons are created through the interaction of the charged particle with the chamber gas in the drift region and the electrons are amplified by the electron avalanche process which occurs at high electric field in GEM holes. The GEM is the double-side printed circuit board, which consists of low temperature co-fired ceramic (LTCC) with 100  $\mu\text{m}$  thickness as an insulator and gold layers with 6  $\mu\text{m}$  thickness on both sides as an electrode. It has also a large number of holes with 100  $\mu\text{m}$  diameter and 200  $\mu\text{m}$  pitch (LTCC-GEM [4]). The LTCC-GEM is quite robust against the large discharge. Fig. 2 shows the experimental setup of the GEM detector. In the clinical practice of the BNCT, a collimator with a diameter of 120 mm is normally used. In this study, the irradiation was performed using an additional collimator with smaller aperture than the effective detection area to demonstrate whether the detector can measure the neutron spatial distribution. In addition, the measurements were performed while changing the detector position in order to observe the neutron flux distributions.

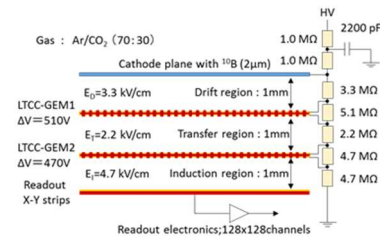


Fig. 1. Cross-section of the GEM detector; electrons are amplified in a succession of steps.

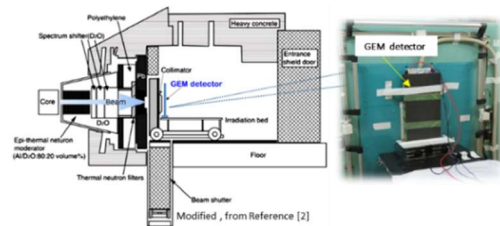


Fig. 2. Schematic diagram of experimental layout and appearance of irradiation geometry at the HWNIF of the KUR.

**RESULTS:** Fig. 3 shows the neutron spatial distribution at a distance of 640 mm from the collimator surface and the horizontal intensity profile at the beam center. The beam condition of the neutron irradiation field could be evaluated in real time and the collimator shape could be clearly seen. Since the detector is not sensitive against gamma-ray, we guess that the tail of the distribution was caused by neutron leaking from the collimator. For pulsed neutron sources, the detector can measure the neutron energy distribution in the time-of-flight method, but for reactor neutron sources, the neutron generation time cannot be determined because neutrons are randomly generated, so the neutron energy distribution cannot be measured. In the future, we plan to make improvements so that the energy distribution of the reactor neutron sources can be evaluated.

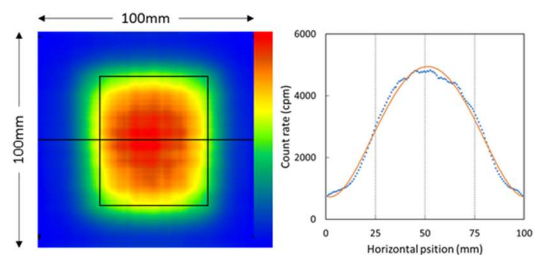


Fig. 3. The neutron spatial distribution and the intensity profile at the beam center. The square black line indicates the collimator size (60 mm  $\times$  50 mm).

### REFERENCES:

- [1] F. Sauli, Nucl. Instrum. Meth., A **386** (1997) 531.
- [2] Y. Sakurai *et al*, Nucl. Instrum. Meth., A **453** (2000) 569.
- [3] S. Uno *et al*, Physics Procedia **26** (2012) 142.
- [4] K.Komiya *et al*, J. Jpn. Soc. Prec. Eng., **84**.11 (2018) 936.

## PR5-18 Development of Epi-thermal Neutron Flux Intensity Detector for BNCT

I. Murata, K. Aoki, Y. Miyaji, S. Kusaka, H. Tanaka<sup>1</sup>, Y. Sakurai<sup>1</sup> and T. Takada<sup>1</sup>

Graduate School of Engineering, Osaka University  
<sup>1</sup>Institute for Integrated Radiation and Nuclear Science, Kyoto University

**INTRODUCTION:** BNCT is a promising cancer therapy which kills tumor cells while suppressing exposure dose to normal tissues. Normally, BNCT neutron field, produced by a nuclear reactor or an accelerator-based neutron source, has energy distribution spreading within thermal, epi-thermal and fast neutron region. Because epi-thermal neutrons ( $0.5 \text{ eV} < E_n < 10 \text{ keV}$ ) are generally used for BNCT, we must measure the epi-thermal neutron flux intensity to evaluate therapeutic effect and patients' exposure dose. However, it is quite difficult to measure it directly and accurately because there is no available method to measure the neutron spectrum and no activation materials covering only epi-thermal region. The objective of this work is hence to design a new detector to precisely measure the absolute integral flux intensity of epi-thermal neutrons.

**EXPERIMENTS:** The present epi-thermal neutron detector needs to reduce sensitivities to thermal and fast neutrons by using cadmium and polyethylene. We carried out numerical simulations by MCNP5. As a result,  $^{71}\text{Ga}$  ( $n, \gamma$ )  $^{72}\text{Ga}$  reaction was selected as the activation detector and the shape of the epi-thermal neutron detector was fixed to be a rectangular polyethylene (5.52 cm cubic) covered with a cadmium sheet (Fig.1). The epi-thermal neutron detector is however a little sensitive to fast neutrons (Fig.2). In order to test the performance of the epi-thermal neutron detector, a verification experiment was conducted at KUR. After the experiment, we can know the epi-thermal neutron flux intensity by Eq. (1). All we have to do is to measure radioactivity of  $^{72}\text{Ga}$ , meaning it is easy and it takes a short time.

$$\Phi_{\text{epi}} = \frac{Q}{Y \times (1 - e^{-\lambda t_1})} \quad (1)$$

$\Phi_{\text{epi}}$ [n / cm <sup>2</sup> / sec]	epi-thermal neutron flux intensity
Q [Bq]	$^{72}\text{Ga}$ radioactivity
Y [atoms / (source_neutron / cm <sup>2</sup> )]	$^{72}\text{Ga}$ production sensitivity
$\lambda$ [1 / sec]	decay constant of $^{72}\text{Ga}$
$t_1$ [sec]	irradiation time

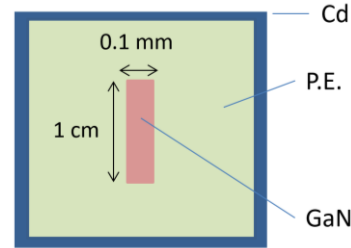


Fig. 1. Calculation model.

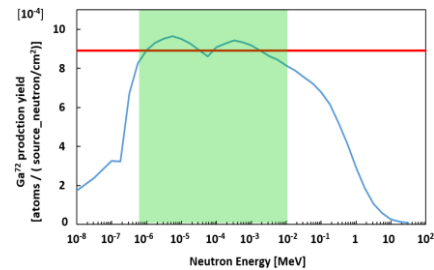


Fig. 2. Sensitivity of epi-thermal neutron detector.

**RESULTS:** Measurement conditions are shown in Table. 1. The radioactivity immediately after irradiation of GaN obtained by the experiment was 1.31 kBq. Therefore, the epi-thermal neutron flux intensity is estimated to be  $1.76 \times 10^8 \text{ n/cm}^2/\text{sec}$  by using Eq. (1). The nominal value of epi-thermal neutron ( $0.5 \text{ eV} < E_n < 10 \text{ keV}$ ) flux intensity is estimated to be  $1.62 \times 10^8 \text{ n/cm}^2/\text{sec}$ . Because this detector is a little sensitive to fast neutrons, it is probable that a discrepancy seen between the experimental value and the nominal value.

To investigate the contribution from fast neutrons, we carried out a correction calculation by MCNP5. As a result, the amount of activation by fast neutrons was estimated to be 50 Bq. Removing the contribution from fast neutron, the radioactivity becomes 1.26 kBq. Then, the epi-thermal neutron flux intensity is finally estimated to be  $1.69 \times 10^8 \text{ n/cm}^2/\text{sec}$ . It shows an excellent good agreement of  $\sim 4\%$ .

Table. 1. Measurement conditions.

Measuring Equipment HP-Ge detector	
Irradiation Time	10 min
Cooling Time	26 min
Measuring Time	55 min
Equipment Efficiency	0.00383741

**CONCLUSION:** The epi-thermal neutron flux intensity could be measured with an error of 4.2 % by correcting with the calculated value in the experiment at KUR. In order not to carry out a correction, we are developing a fast neutron ( $10 \text{ keV} < E_n < 1 \text{ MeV}$ ) flux intensity detector.

## PR5-19 Investigation of Thermal Neutron-Induced Soft Errors in Semiconductor Devices

H. Tanaka, T. Kato<sup>1</sup>, H. Matsuyama<sup>1</sup> and T. Takata and Y. Sakurai

*Institute for Integrated Radiation and Nuclear Science, Kyoto University*  
*<sup>1</sup>Reliability and Quality Assurance Department, Socionext Inc.*

**INTRODUCTION:** Soft errors are radiation-induced errors in semiconductor devices. Although the soft errors can be recovered by reset or power cycle of the devices, this is a critical issue in high reliability applications, such as automated driving and factory automation.

In the terrestrial environment, the major radiation source for the soft error is cosmic-ray-induced neutrons. The energy spectrum of the terrestrial neutron ranges from thermal to high-energy (GeV). The semiconductor device is sensitive to the thermal neutrons when it contains a number of <sup>10</sup>B atoms. The key mechanism is neutron-induced <sup>10</sup>B fission, which produces He and Li ions. These ions deposit charges in transistors, leading to the occurrence of the soft errors [1].

Historically, the thermal neutron-induced soft errors were suppressed by eliminating a borophosphosilicate glass (BPSG) layer, which contained <sup>10</sup>B atoms. However, in recent semiconductor devices, the thermal neutron sensitivity reappeared due to a change in the manufacturing process [2, 3]. Therefore, it is important to explore the thermal neutron sensitivity in advanced devices.

In this study, the thermal neutron-induced soft errors are investigated by irradiation testing. Soft error rates (SERs), which are the occurrence rates of radiation-induced error events, are statistically analyzed in advanced static random access memories (SRAMs).

**EXPERIMENTS:** Irradiation tests were performed using Heavy Water Neutron Irradiation Facility (HWNIF) of KUR [4]. The irradiation mode was “OO-0000F.” Fig. 1 shows the energy spectrum of this mode (black solid line) together with that of the terrestrial environment (gray dashed line) [5]. It is seen that these two spectra are similar to each other. In other words, this neutron source is suitable for the accelerated test of the terrestrial neutron-induced soft errors.

The samples were SRAM chips manufactured in advanced CMOS processes. Two types of SRAM chips, which were labeled as Device A and Device B, were irradiated. The number of error events occurred during irradiation were analyzed. The SERs were then calculated according to the JEDEC standard [6]. To estimate thermal neutron fluxes at the locations of samples, gold wires were attached on the SRAM chips. The fluxes were determined based on the activation of the gold.

Additionally, irradiation tests with boron shields were conducted for Device A. The boron shields were placed surrounding the SRAM chip to attenuate thermal neutrons. To clarify the sensitivity to thermal neutrons, the SERs with and without the boron shields were compared.

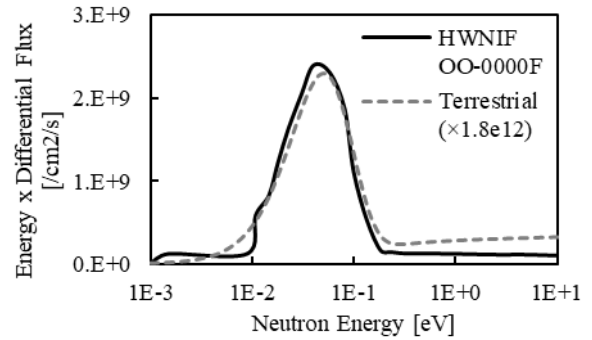


Fig. 1. Neutron energy spectra of HWNIF OO-0000F [4] and terrestrial environment [5]

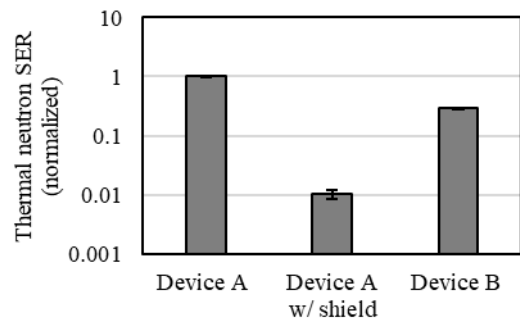


Fig. 2. Thermal neutron SERs of Device A, Device A with boron shield, and Device B.

**RESULTS:** Fig. 2 presents the thermal neutron SERs of Device A and Device B, where the SER values are normalized by the value of Device A. As for Device A, the SER with the boron shields is also shown.

In the comparison between the SERs of Device A with and without the boron shields, it was demonstrated that the SER with the shields was significantly reduced by two orders of magnitude.

As for the comparison between Device A and Device B, the SER of Device B was lower by 70%. This is probably due to the difference in the manufacturing process between them.

We have demonstrated that the advanced SRAMs are sensitive to thermal neutrons and that the SERs are different device-to-device, indicating the importance of thermal neutron irradiation testing.

### REFERENCES:

- [1] R. Baumann *et al.*, Proc. IEEE Int. Reliab. Phys. Symp. (IRPS), 152 (2000).
- [2] S. Wen *et al.*, Proc. IEEE Int. Reliab. Phys. Symp. (IRPS), SE.5.2 (2010).
- [3] Y. Fang *et al.*, IEEE Trans. Device Mater. Rel., **14**, 583 (2014).
- [4] Y. Sakurai *et al.*, Nucl. Instr. Meth. A, **453**, 569 (2000).
- [5] T. Sato, PLoS ONE, **10(12)** (2015).
- [6] JEDEC Standard JESD89A (2006).